Article:
Brown, B., Ward, A., Fazili, Z. et al. (2021) Application of UV dissolution imaging to pharmaceutical systems. Advanced Drug Delivery Reviews, 177. 113949. ISSN: 0169-409X

https://doi.org/10.1016/j.addr.2021.113949

Advanced Drug Delivery Reviews 177 (2021) 113949

Contents lists available at ScienceDirect

Advanced Drug Delivery Reviews

journal homepage: www.elsevier.com/locate/adr

Application of UV dissolution imaging to pharmaceutical systems ☆

Benedict Brown [a,b], Adam Ward [a,b], Zayeem Fazili [a,b,c], Jesper Østergaard [d], Kofi Asare-Addo [a,*]

[a] Department of Pharmacy, University of Huddersfield, Huddersfield HD1 3DH, UK
[b] EPSRC Future Metrology Hub, University of Huddersfield, Huddersfield HD1 3DH, UK
[c] Department of Computing and Engineering, University of Huddersfield, Huddersfield HD1 3DH, UK
[d] Department of Pharmacy, University of Copenhagen, Universitetsparken 2, DK-2100 Copenhagen O, Denmark

ARTICLE INFO

Article history:
Received 23 April 2021
Revised 11 August 2021
Accepted 23 August 2021
Available online 28 August 2021

Keywords:
Diffusion
Dissolution testing
Intrinsic dissolution rate
In-vitro release
Parenterals
UV imaging

ABSTRACT

UV–vis spectrometry is widely used in the pharmaceutical sciences for compound quantification, alone or in conjunction with separation techniques, due to most drug entities possessing a chromophore absorbing light in the range 190–800 nm. UV dissolution imaging, the scope of this review, generates spatially and temporally resolved absorbance maps by exploiting the UV absorbance of the analyte. This review aims to give an introduction to UV dissolution imaging and its use in the determination of intrinsic dissolution rates and drug release from whole dosage forms. Applications of UV imaging to non-oral formulations have started to emerge and are reviewed together with the possibility of utilizing UV imaging for physical chemical characterisation of drug substances. The benefits of imaging drug diffusion and transport processes are also discussed.

Contents

Abbreviations: API, Active Pharmaceutical Ingredient; ASD, Amorphous Solid Dispersion; UV, Ultra-Violet; CARS, Coherent Anti-Stokes Raman Scattering Microscopy; MRI, Magnetic Resonance Imaging; FaSSGF, Fasted State Simulated Gastric Fluid; FeSSIF, Fed State Simulated Intestinal Fluid; FTIR, Fourier Transforms Infrared; FVM, Focus Variation Microscope; CLSM, Confocal Laser Scanning Microscopy; NMR, Nuclear Magnetic Resonance; THz, Terahertz; NIR, Near Infra-red; XμT, X-ray micro-Tomography; PAT, Process Analytical Tools; SEM, Scanning Electron Microscope; CMOS, Complementary Metal Oxide Semiconductors; CCD, Charged Coupled Devices; GIT, Gastro-Intestinal Tract; DIDR, Disk Intrinsic Dissolution Rate; BCS, Biopharmaceutics Classification System; MCC, Microcrystalline Cellulose; SDS, Sodium Dodecyl Sulfate; PCL, Poly-ε-Caprolactone; SDI, Surface Dissolution Imaging; HPC, Hydroxypropylcellulose; LOQ, Limit of Quantification; pI, Isoelectric Point.

☆ This review is part of the Advanced Drug Delivery Reviews theme issue on "Emerging Technologies".

* Corresponding author.
E-mail address: k.asare-addo@hud.ac.uk (K. Asare-Addo).

https://doi.org/10.1016/j.addr.2021.113949
0169-409X/

1. Introduction

Traditional drug dissolution and release testing methods are based on measurements of the active pharmaceutical ingredient (API) in the bulk solution or in samples withdrawn from the medium, which upon accumulation often is analysed by a UV spectrophotometric technique. The measurement approaches may be intrusive and disturb the release process without offering significant insights into drug release mechanisms. Thus, there has been a drive towards real-time analysis and continuous monitoring methods to determine and better understand dissolution and drug release phenomena. This has led to utilization of fibre optic UV probes and the implementation of advanced imaging techniques in dissolution and release testing.

Advanced imaging techniques applied within the pharmaceutical industry can provide useful real-time information to understand critical behaviour of APIs. Imaging techniques that have found use in drug development include Coherent Anti-Stokes Raman Scattering Microscopy (CARS) [1], Raman spectroscopy and imaging [2,3], Magnetic Resonance Imaging (MRI) [4,5], X-ray micro-Tomography (XμT) [6], Fourier Transform Infrared (FTIR) imaging [7,8], Near Infra-red (NIR) imaging [9,10], fluorescence imaging [11], Terahertz (THz) imaging [12,13], Confocal Laser Scanning Microscopy (CLSM) [14], and UV dissolution imaging [15,16].

Briefly, CARS has been used in the imaging of the solid-state changes of APIs *in situ* in dissolution to correlate with dissolution rate change [1,17] the release of API from pharmaceutical tablets [18]. Raman imaging has been used to assess excipient distribution within a tablet [19,20] for chemical imaging of nasal spray suspensions and API distribution within a tablet [21,22]. NMR/MRI has been used to study the internal mechanisms of the *in vitro* drug release in dosage forms such as the ingress of dissolution media [23,24,25,26,27], water distribution in extrudates [28], water diffusion coefficients and polymer concentrations [29,30,31,32], water penetration in osmotic pumps [33], homogeneity in powder mixtures [34], the tablet disintegration process [35], internal barriers for zero-order release systems [36], pulsatile capsules [37] and mapping the distribution of porosity in compacts [38]. XμT has been used to measure/assess heterogeneity of powder beds [39,40], density variations in compacts [41,42] with and without embossed features [43,44], porosity of hot-melt extrudates [45], compression characteristic of dry coated tablets [46], packing in granular systems [47,48], excipient homogeneity [49], visualization of tablets after drug release [50]. FTIR imaging has allowed dissolution studies of tablet-in-tablet formulations [51], within-tablet dynamics for extended release formulations [52] and pharmaceutical films [53]. The depletion of API and the hydration processes for hydrophilic matrices [54,55,56] as well as films [57] and pharmaceutical product characterisation [58] have been visualised using NIR imaging. Fluorescence imaging has been applied to the swelling of polymers to investigate molecular diffusion and interactions between chromophores and solvent molecules [59 60,61,62]. Recent developments in semiconductor physics and ultrafast laser technology have made it possible to provide light at terahertz frequencies which now allow the analysis of coating thickness, structure and uniformity and intra-tablet coating uniformity [12,63,64,65,66,67], chemical component calibration and density mapping [68,69,70], inspection of pharmaceutical tablets and quality control [71,72], dissolution assay for immediate-release tablets [73], and determining porosity and non-contact weight measurements [74,75,76]. CLSM has been utilised in a number of different pharmaceutical applications such as the visualisation of the early gel layer formation in tablet matrices [77,78], visualisation and identification of the percolation threshold [79], visualisation of drug release from milk and fat-rich emulsions [80] and the designing of matrices with improved resistance to dissolved sugar and dietary sugars [78,81]. Optical microscopy has also been used to visualise and determine intrinsic dissolution rates (IDRs) from single drug particles as small as 14 μg [82,83,84] These methodologies have wide-ranging applications from the early drug development phase, characterisation of drug delivery systems, process measurements, as process analytical tools (PAT), product performance testing and quality control.

UV dissolution imaging is an emerging technology that provides visualisation of the dissolution of a material and subsequent related events at the solid-liquid interface as well as obtaining a concentration measurement. The insights offered into API behaviour will be useful in providing an understanding for phenomena not usually captured in offline measurements. UV dissolution imaging, sometimes referred to as UV imaging, UV/Vis imaging or surface dissolution imaging, has offered a compound sparing approach to the determination of IDRs. However, additional UV imaging applications in relation to oral as well as non-oral formulations and physical chemical characterization have started to occur. Here we aim to give an introduction to UV dissolution imaging covering the basic principles of the technology as well as current applications to pharmaceutical systems, hoping to spur new ideas and widen uptake in pharmaceutical research. The review addresses visualization of dissolution phenomena in relation to form selection, to determination of intrinsic dissolution rates, and to drug-excipient compatibility in early drug development. These relatively best-established applications of UV dissolution imaging, are followed by drug release studies from whole dosage forms, which have become available due to recent instrumentation developments. Likewise, applications of UV imaging to non-oral formulations are starting to emerge and are reviewed together with the utilization of UV imaging for physical chemical characterization of drug substances. Advantages and limitations of the technology are discussed with a perspective to the positioning of UV imaging relative to more advanced imaging modalities used in drug development.

2. Principles of UV imaging

Most pharmaceutically relevant applications of the UV/Vis spectrophotometry is based on light in the wavelength range 190 nm to 800 nm, with UV light ranging from 190 to 400 nm and visible light from 400 to 800 nm [85,86]. The ability of drug substances to absorb light forms the basic principle of UV/Vis spectrophotometry and UV/Vis imaging. The absorption takes place

when an electron is promoted to a higher energy state by the energy of an incident photon where the extent of the light absorbed by the compound in the UV/Vis spectrum is determined by the chromophores present in the molecule. The main application of spectrophotometry is quantification of compounds present in solution. However, different molecular structures will yield different absorbance spectra, which may be useful as a secondary method in compound identification [86]. The quantification is governed by absorbance of light according to the Beer-Lambert law (Equation (1)) stating that the amount of light absorbed is directly proportional to the concentration of absorbing species present in the medium.

$$\log_{10}\left(\frac{I_0}{I}\right) = \log_{10}\left(\frac{1}{T}\right) = A = \varepsilon bc \quad (1)$$

where I_0 denotes the incident light intensity, I is transmitted light intensity, T specifies transmittance given by $\frac{I}{I_0}$, b is the light path, A is the absorbance, ε is the molar absorption coefficient, and c denotes the concentration of the absorbing substance.

The Beer-Lambert's law only applies to monochromatic radiation. However, in practice, polychromatic radiation is applied, which may cause deviation from the Beer-Lambert's law [85,86,87]. Other causes for deviation from the Beer-Lambert law relate to the instrumentation, for instance stray light or may be attributed to properties of the analytes. High analyte concentrations may lead to refractive index changes, chemical reactions, self-association or interactions between molecules (e.g., drug – surfactants interactions) in solution can lead to deviations from linearity. Given the absence of interactions affecting the absorbance spectra, the Beer-Lambert law applies to mixtures of molecules or analytes. This and, in particular, the proportionality, between absorbance and concentration, make UV/Vis spectrophotometry and imaging convenient and relatively simple means for quantification of drugs. Spatially and temporally resolved absorbance measurements are used in the creation of images from UV (and Vis) imaging [16,88].

2.1. UV imaging instrumentation

The UV imaging systems encountered in this review utilises a CMOS based image detector to record images. The application of a phosphor coating produces a spectra shift from 200 to 400 nm into the visible range and thus allowing detection [89]. Limitations for conventional CMOS detectors include higher noise, lower image quality, lower sensitivity and a limited dynamic range, however the recent development CMOS detectors has addressed many of these limitations, making CMOS detectors suitable for scientific applications, which can perform well in the UV range [90,91]

The earliest applications of UV imaging were in the area of separation sciences, electrophoretically mediated microanalysis and capillary electrophoresis, using the Paraytec Actipix D100 detector [92,93,94,95]. Quartz cells were developed for the imaging detector allowing development of pharmaceutical applications [96]. The design of the imaging system and the relatively small imaging area (7×9 mm^2) was suited for compound sparing small-scale dissolution studies, leading to IDR measurements to be among the first applications to emerge [97,98]. Recent developments have been in the direction of larger imaging areas and multi wavelength imaging allowing studies of larger and more complex samples [16]. The interested reader can get an appreciation of the commercial instruments iterations that have occurred and instrument specifications from Table 1 and the literature [16,99,100,101]. Taking into account that different instruments are available and assuming further instrument developments, the description of UV dissolution imaging instrumentation below is limited to a generic level.

Table 1
System overview of the commercially available surface dissolution imaging equipment.

Instrument	Imaging area	Pixel size	Resolution	Light source	Comments
D100	7×9 mm^2	7×7 µm^2	40 µm x-direction 30 µm y-direction [99]	Pulsed xenon flash lamp 190 – 1100 nm via bandpass filter	Standalone CMOS detector
SDI 300 (Also known as SDI or SDI1)	7×9 mm^2	7×7 µm^2	40 µm x-direction 30 µm y-direction [99]	Pulsed xenon flash lamp 190 – 1100 nm via band pass filters	First purpose-built surface dissolution imaging system, using syringe pump
D200	28×28 mm^2	13.75×13.75 µm^2	30 µm (both direction) [102]	LEDs: 255 nm, 280 nm, 320 nm, 525 nm	Standalone CMOS detector
(VARIOUS CONFIGURATIONS)	11×11 mm^2	5.5×5.5 µm^2	ND[a]	Pulsed xenon flash lamp 180–800 nm via bandpass filter	
		5.5×5.5 µm^2	ND[a]		
	11×6 mm^2				
SDI2	28×28 mm^2	13.75×13.75 µm^2	ND [a]	LEDs: 255 nm, 280 nm, 300 nm, 320 nm, 520 nm	Fully integrated system, containing CMOS detector and automated pumps. Compact flow cell and whole dosage cell configurations.

ND[a] - Not experimentally determined.

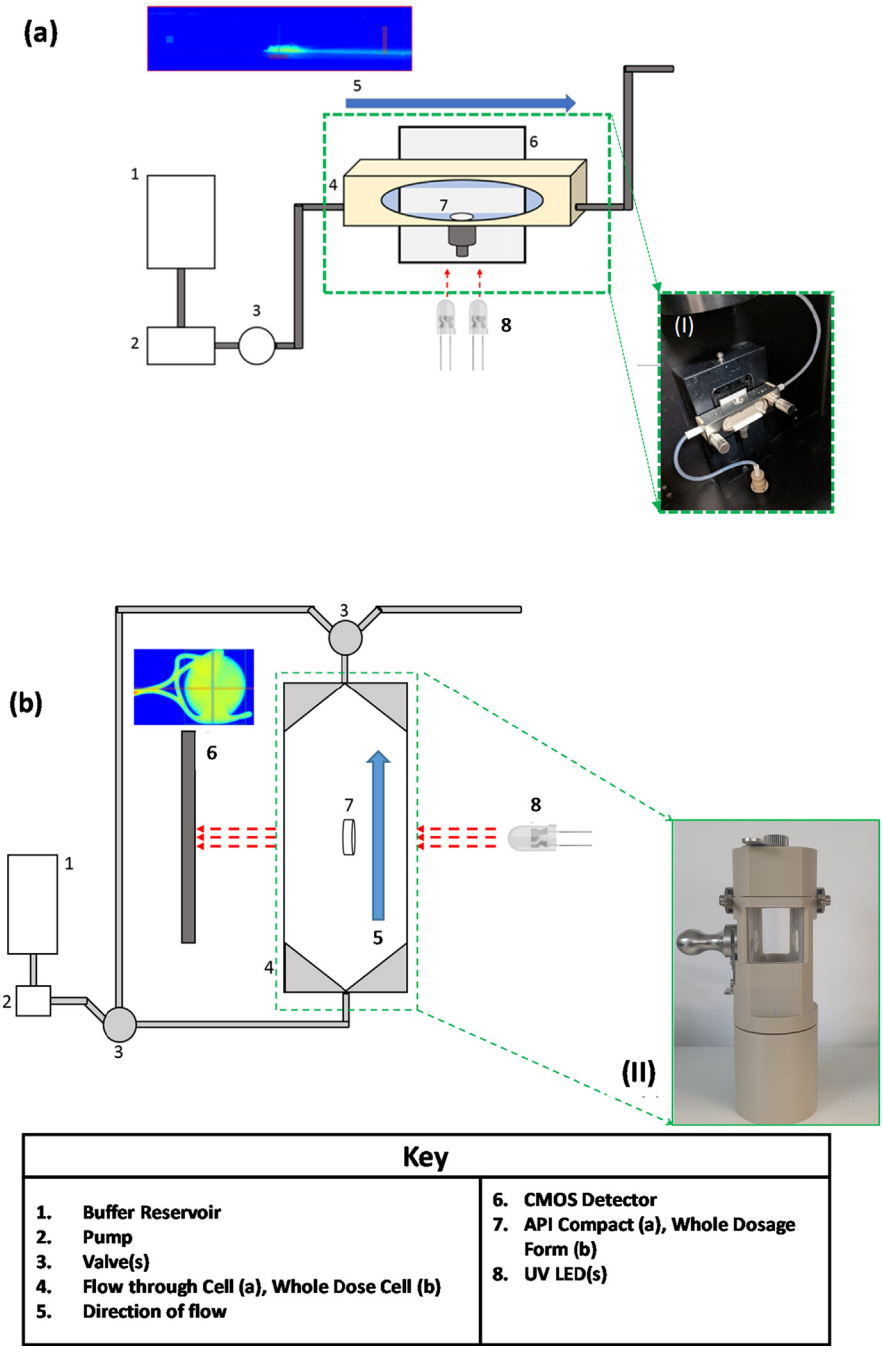

Fig. 1. Schematic representations of a UV imaging system for (a) intrinsic dissolution rate (IDR) measurements and (b) whole dosage form imaging. The photographs (I) and (II) show the Pion SDI2 compact flow cell and (b) whole dose set-up, respectively. The inserts show representative UV images obtained during dissolution testing. The effective image area is 28 × 28 mm^2 and the instrument allows selection of two wavelengths at a time: 255, 280, 300, 320, and 520 nm [108]. Reprinted from [105]. Copyright (2019) with permission from Elsevier.

The key components of a UV dissolution imaging system are a light source, a quartz cell for containing the sample of interest and an imaging detector (Fig. 1). The system has to be shielded from outside light because the phosphor coated CMOS chip is sensitive to light in both the UV and Vis wavelength range. Wavelength selection is achieved by LEDs emitting light of a narrow wavelength range or the use of band pass filters in conjunction with a pulsed Xenon lamp. Key distinguishing features between early instrumentation and more recent instruments are the size of the imaging area (currently up to 28 × 28 mm^2, 2048 × 2048 pixels) and the ability to perform multi wavelength imaging (up to 4 wavelengths) or not. In addition, dedicated cells and pump systems for medium handling differentiate the systems. The schematic in Fig. 1 shows the most typical configurations for a UV imaging system (Pion SDI2) with two different flow cells, the so called compact cell (Fig. 1a) and the whole dose cell (Fig. 1b) to image compacts (IDR determinations) and formulated full dosage forms, respectively. The compact cell is specifically designed to image compacts made from API powders to determine the intrinsic dissolution rate (IDR). The design of this cell resembles the classical Nelson and Shah cell [103], providing laminar flow condition across a solid surface of compacted material (3–10 mg). The whole

dose cell is based on a USP apparatus IV-like flow cell used to image dissolution and release of API from whole dosage forms such as tablets and capsules [104,105,106,107]. The cell is cylindrical (Fig. 1b) with dimensions 142.5 mm × 27.5 mm (H × D) with a conical shape which holds glass beads, has a volume of 60 mL. The imaging area is 28 mm × 24 mm^2 (H × W) and optical path length is variable ≤ 28 mm due to the cylindrical shape [108].

3. Small-scale dissolution and intrinsic dissolution rate measurements

Dissolution testing commonly constitutes a significant element of more or less complex setup designed to mimic the physiology of the gastrointestinal tract (GIT). Reviews of existing *in-vitro* models for predicting *in-vivo* performance suggest that there is no one method that can fit all needs with respect to the methodology chosen. Methodology chosen can be dependent on factors such as requirements for the development phase and the drug delivery system [109,110,111].

Most of the traditional or conventional *in-vitro* dissolution methods such as the rotating disc, paddle, and basket methods often require relatively larger amounts of dissolution medium, API or formulation. Due to the limited amount of API present during the early stages of drug development, miniaturised or micro-dissolution techniques that require only few milligrams of the API are of interest as they do overcome some of these limitations [97,111,112,113,114,115,116]. This drive towards miniaturisation has produced instrumentation that uses either offline or real-time analytics, including the mini-paddle apparatus [117,118], mini dissolution vessel [119], 96-well plate assay for intrinsic dissolution testing (MINIDISS) [120], transfer method to predict precipitation [121], solvent shift method [122], μDISS using UV fibre optics [112], miniaturised rotating disk intrinsic dissolution test [115], μFlux test [123], Partially Automated Solubility Screening (PASS) assay [124], miniaturized assay for solubility and residual solid screening (SORESOS) [125], SiriusT3 and inForm [111], and UV dissolution imaging [97,98,126]. The advantage of these miniaturised techniques is that they are classed as compound-sparing meaning each IDR determination typically requires 5–10 mg of sample, or less. This compares favourably to traditional IDR determinations such as the Woods apparatus, which often requires in the order of hundreds of milligrams of an API. Thus, IDR determination via a miniaturised method is an attractive option in the early stages of development, where when access to API often is limited.

Solid drugs have been characterised using disk intrinsic dissolution rate (DIDR) for many years [112,127,128]. As DIDR is a rate phenomenon and not an equilibrium phenomenon, it is thought to correlate more closely with *in-vivo* drug dissolution dynamics than solubility. Consequently, it has been suggested that DIDRs be used to classify drugs instead of solubilities as used in the Biopharmaceutics Classification System (BCS) [129].

Intrinsic dissolution rate (IDR) is defined as the rate of mass transfer per a unit area which is exposed to dissolution media [130]. Throughout an experiment, the IDR surface area should be kept constant, and the use of a constant flow of dissolution media (in the case of UV dissolution imaging) applied to maintain sink conditions.

The pharmacopoeia method described for IDR determinations include the rotating disk system (or Wood's apparatus). The IDR, which is expressed by the Nernst-Brunner's adaptation of the Noyes-Whitney equation and commonly obtained from the modified USP I/II set up, takes into consideration the concentration of the API dissolved, sampling time, diffusion coefficient, surface area, volume of the medium, boundary layer thickness, and the concentrations at saturation at the solid surface and in the bulk solution [131].

The Nernst-Brunner and Noyes-Whitney equations constitute a convenient frame for the discussion of dissolution processes (occurring in vessels or vials). For flow-through based UV dissolution imaging, however, the convective diffusion drug dissolution model developed by Nelson and Shah [132,103,133], serves as the quantitative basis. The dissolution rate (R) is represented by Equation (2) according to the convective diffusion dissolution model in case of a circular compact. Using the model of Nelson and Shah and taking into account the two-dimensional images captured by UV imaging, IDR values may be calculated according to Equations (3) and (4) [133].

$$R = 2.157 \cdot D^{\frac{2}{3}} \cdot c_0 \alpha^{\frac{1}{3}} \cdot r^{5/3} \tag{2}$$

$$IDR = \frac{\sum_{z=0}^{\frac{H}{2}} (v_z M c_z W \Delta_z)}{S} \tag{3}$$

$$vz = \frac{3Q}{2HW} \cdot \left(1 - \left(\frac{\left(2z - H^2\right)}{H^2}\right)\right) \tag{4}$$

where D is the diffusivity, c_0 is the solubility and r is the compact radius, z is the height above the z-origin, v_z is the velocity at z, M is the molecular weight, c_z is the concentration at z, W is the width of flow cell channel, Δz is the effective pixel height, S is the surface area of sample, H is the height of flow cell channel in the observation region and Q is the volumetric flow rate [133].

3.1. Characterisation techniques used with UV dissolution imaging

The dissolution behaviour of an API is intimately related to its solid-state properties. A comprehensive characterisation of the solid form properties is essential because drugs may have a propensity to undergo solvent mediated solid form transitions during dissolution experiments [97,134,135,136]. It is therefore commonplace to characterise the solid-state properties of compound, prior to IDR determination. Most studies achieve this via the use of in-situ or offline Raman spectroscopy, differential scanning calorimetry (DSC), X-ray powder diffraction (XRPD), scanning electron microscopy (SEM) and focus variation microscopy (FVM) (Table 2).

One area of particular success is the ability to assess the interplay between solvent mediated solid form transitions and drug dissolution [97,134,135,136] (Table 2). A few studies have reported the use of *in-situ* Raman spectroscopy measurements and UV dissolution imaging data to be collected simultaneously [137,136,138]. Scanning electron microscopy (SEM) or optical microscopy have been used to qualitatively assess the quality of the drug compacts prior to IDR determinations. The need to generate quantitative data describing surface properties of the compacts used for IDR determinations has also spurred the incorporation of focus variation microscopy (FVM) as a tool for characterizing surface topography [139,140]. This technique, which stems from the field of precision engineering, has the ability to accurately measure the surface topography of drug compacts. This allowed for the exploration of how manufacturing conditions affected the surface of the drug compacts and how the dissolution process itself changed the topography of the drug compact [139,140].

3.2. UV dissolution imaging and IDR determination

A typical image generated by a UV imaging dissolution instrument is depicted in Fig. 2. The dissolution of indomethacin is apparent as the increase in absorbance at 320 nm. The indomethacin

Table 2
Application of UV dissolution imaging in intrinsic dissolution rate (IDR) measurements and drug-excipient compatibility studies.

Drug/ excipient	Comments	Physical characterisation	Complementary assessment	Reference
Amlodipine	Solvent mediated solid form transformation	DSC, TGA, NMR, XRPD	Raman spectroscopy*, optical microscopy	[97]
Danirixin	Reduced pharmacokinetic variability in patient populations using salt forms of Danirixin	–	–	[148]
HPMC	HPMC swelling behaviour	–	Optical microscopy	[176]
Indomethacin, theophylline, ibuprofen	Effects of particle size, salt and polymorphic forms	XRPD, IR spectroscopy, DVS	Raman spectroscopy*	[98]
Carbamazepine–Nicotinamide cocrystals	Solvent mediated solid form transformation	TGA, DSC, IR spectroscopy	Raman spectroscopy*, SEM, optical microscopy	[134]
Paracetamol	Computational dissolution simulation in conjunction with physical experiments	–	–	[141]
Furosemide	Salt disproportionation	TGA, XRPD, IR spectroscopy	Raman spectroscopy*	[135]
Indomethacin	Dissolution of nanocrystals	DSC	SEM	[170]
Furosemide	Biorelevant media and impact of flow rate	XRPD	Raman spectroscopy*	[151]
Carbamazepine–Nicotinamide Cocrystal	Influence of SDS and Tween 80 on dissolution	DSC, IR spectroscopy	Raman spectroscopy*, optical microscopy	[142]
Celecoxib, ketoprofen, naproxen, sulfathiazole	Analysis of early stage dissolution kinetics	DSC, XRPD	Raman spectroscopy*, SEM	[143]
Naproxen, theophylline	Solvent mediated solid form transformation	XRPD	In-situ Raman spectroscopy*	[136]
Naproxenate sodium	Microenvironmental pH measurements during dissolution	–	–	[144]
Albendazole, celecoxib ezetimibe, furosemide, glibenclamide, indomethacin, ketoprofen mebendazole, mefenamic acid, naproxen, phenytoin probucol, sulfasalazine sulfathiazole	Dissolution of 1:1 solid dispersions with either mono or diacyl lecithin phospholipid	DSC, XRPD	Optical microscopy	[188]
Nilotinib	pH mediated swelling of nilotinib-polymer dispersions	DSC, IR spectroscopy, WAXS	In-situ Raman spectroscopy*	[137]
Carbamazepine, ibuprofen	Solvent mediated solid form transformation	–	–	[193]
Lidocaine single crystal	Assessment of instrument performance (SDI and D100)	–	–	[99]
Grisefulvin	Dissolution - SDS solid dispersions	–	SEM-EDX	[192]
Ibuprofen	Surface topography using FVM	DSC, XRPD	FVM	[139]
Fenofibrate	Impact of drug nanocrystallisation on drug release from oral strip-films	DSC, TGA, XRPD, IR spectroscopy	Raman spectroscopy*, SEM	[175]
Fenofibrate	Sustained release from hydrophilic polymeric film sandwiched between hydrophobic layers	XRPD, TDA, ATR-FTIR	FE-SEM	[174]
Theophylline	Fragmentation and release from 3D printed cellulose tablets	DSC, TGA	SEM, XμCT	[177]
Gemfibrozil	Effect of salt formation	DSC, XRPD	FVM, SEM	[194]
Acetylsalicylic acid	Effects of excipient shielding on dissolution	Solution calorimetry	Raman spectroscopy*, optical microscopy	[191]
Cefuroxime axetil, itraconazole	Effect of solid forms (amorphous)	–	–	[190]
Indomethacin	Drug – Soluplus solid dispersions	DSC, XRPD	FVM, SEM	[105]
Paracetamol, carbamazepine	Effect of superdisintegrants	–	–	[189]
Bromocriptine mesylate, carvedilol, ibuprofen, indomethacin, tadalafil, valsartan	Interlaboratory study	–	–	[130]
Naproxen, sodium naproxen	Dissolution of co-amorphous system, solid forms	DSC, XRPD, IR spectroscopy	In-situ Raman spectroscopy*	[138]
Ibuprofen, ketoprofen, paracetamol	Effects of drug compact topography	XRPD	FVM	[140]

Note: XμCT = X-ray micro-Computed Tomography, XRPD = X-ray Powder Diffraction. DSC = Differential Scanning Calorimetry, FVM = Focus Variation Microscopy, IR = Infra-Red, SEM = Scanning Electron Microscopy, FE-SEM = Field Emission Scanning Electron Microscopy, TGA = Thermogravimetric Analysis, NMR = Nuclear Magnetic Resonance, DVS = Dynamic Vapour Sorption, WAXS = Wide-Angle X-ray Scattering, ATR-FTIR = Attenuated Total Reflectance-Fourier Transform Infrared

* signifies not an imaging technique

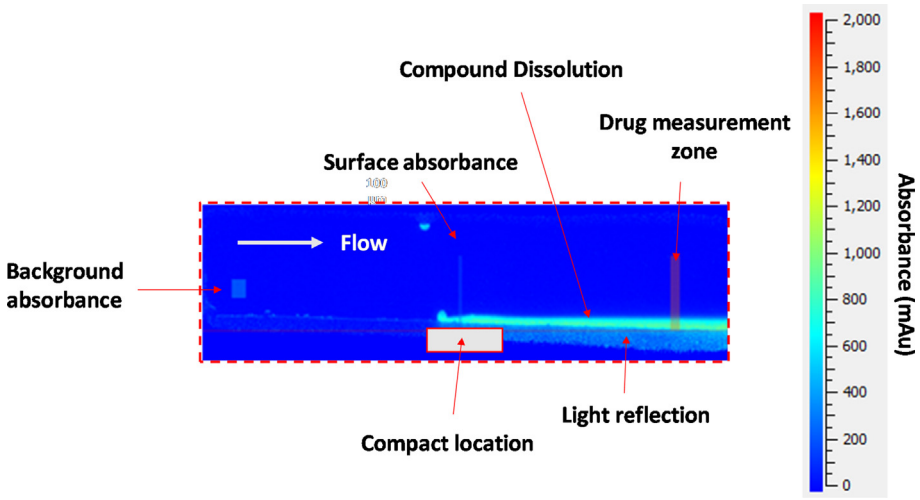

Fig. 2. Image from the analysis software of the UV dissolution imaging instrument (Pion SDI2). The image shows the dissolution of indomethacin from solid compact into phosphate buffer (pH 7.2) at a flow rate of 2 mL/min at 37 °C. Detection at 320 nm. Modified and reprinted from [105]. Copyright (2019) with permission from Elsevier.

dissolved from the compact is carried with the flow exiting the flow cell on the right hand side (Fig. 2). The flow conditions appear to be laminar. The swelling and dissolution-precipitation phenomena that some substances are subject apparently did not occur under the experimental conditions applied. As mentioned above, quantitative information may be extracted from the images captured. Data analysis software typically allows for correction of changes in medium absorbance (reference zone), measurement of the drug concentration immediately above the compact surface using the so-called surface absorbance zone, and quantification of the amount of drug dissolved per area and time unit from the IDR absorbance zone (Fig. 2). The software also allows additional absorbance measurement zones to be positioned in any area within the image field. The IDR is calculated from the model and equations presented in Section 3. Consequently, IDR measurements by UV imaging are prone to error when the hydrodynamic model does not match the actual flow conditions, for instance, due to density effects, gelling or swelling of the API or precipitated material affecting the hydrodynamic pattern, or when the Beer-Lambert law is not adhered to [141,136].

3.2.1. Polymorphs, salts and form selection

The application of flow-through UV dissolution imaging for dissolution studies was first proposed by Wren and Lenke [96]. The first study to report intrinsic dissolution rates was performed on amlodipine besylate [97]. Two amlodipine besylate forms (amorphous and dihydrate) as well as the free base form were subjected to UV dissolution imaging in combination with off-line Raman spectroscopy measurements. The IDRs were in the order amorphous amlodipine besylate > amlodipine besylate dihydrate > amlodipine free base. The decrease in the IDR of the amorphous form observed was due to a solvent mediated solid form transition as confirmed by Raman spectroscopy. During dissolution, API swelling or recrystallization at the compact surfaces (the amorphous and free base forms) was visualized and recorded by UV imaging in real time [97] (Fig. 3 I and II).

Li and co-workers expanded the application of UV imaging dissolution to pharmaceutical cocrystals using carbamazepine as the API of interest and nicotinamide as the cocrystal former [134,142]. Qiao et al. utilised UV imaging to gain an understanding of the intrinsic dissolution behaviour of carbamazepine-nicotinamide cocrystals [134]. For comparison, dissolution studies were conducted on carbamazepine dihydrate, carbamazepine forms I and III, nicotinamide as well as a physical mixture of carbamazepine and nicotinamide. Each sample was subjected to SEM analysis at various points with attempts made to visualise the dissolution effects on the sample surface topography. Offline Raman spectroscopy was used to evaluate solution mediated solid form transformations; this showed that the cocrystal, the two polymorphic forms and the physical mixture all underwent conversion to carbamazepine dihydrate during dissolution and that this was associated with a decrease in IDR as determined via UV imaging. Of interest was the slower IDR decrease for the cocrystals as compared to the pure drug and physical mixture. This was confirmed to be due to a slow recrystallisation of carbamazepine cocrystal to carbamazepine dihydrate during dissolution. Qiao et al. demonstrated the ability to monitor dissolution processes over prolonged periods of time (up to 3 h). Most other UV imaging-based dissolution studies followed the dissolution process for 10–20 min [97,98,135,143]. The influence of sodium dodecyl sulfate (SDS) and Tween 80 addition to the dissolution medium below and above the critical micelle concentration on the dissolution of carbamazepine–nicotinamide cocrystals, carbamazepine III, and carbamazepine–nicotinamide physical mixture was investigated [142]. SDS was found to significantly increase the IDR, whereas Tween 80 addition lead to a decrease of carbamazepine IDR from the co-crystal. Characterisation of the solid-form showed solution-mediated solid form transformation into carbamazepine dihydrate to occur during the dissolution process.

Hulse et al. showed how a range of parameters such as the polymorphic form and particle size affected the dissolution of indomethacin, theophylline and ibuprofen [98]. UV imaging was able to successfully distinguish between the dissolution behaviour of alpha and gamma indomethacin, anhydrous and monohydrate theophylline and ibuprofen sodium and free base. Theophylline anhydrate exhibited a higher dissolution rate when compared to its monohydrate form. Sodium ibuprofen was also shown to exhibit a higher rate of dissolution as compared to ibuprofen in phosphate buffer (pH 7.2). When the effects of micronisation of indomethacin were studied, the unmicronised powder, which had larger particles, resulted in a faster dissolution for the alpha indomethacin as compared to the micronized powder. This phenomenon was explained as the change in surface energy due to micronisation bringing about an increase in the proportion of

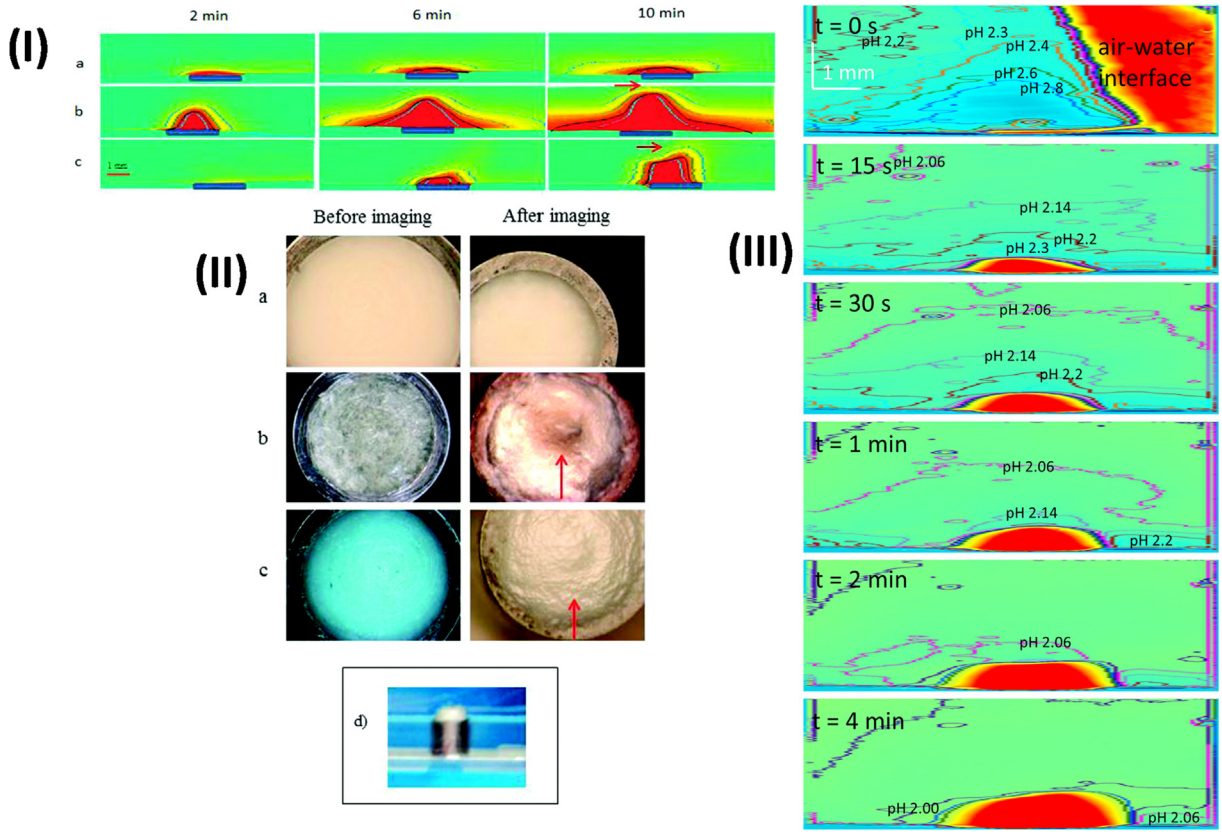

Fig. 3. (I) UV absorbance maps of dissolution at static conditions of (a) amlodipine besylate dihydrate, (b) amorphous amlodipine besylate and (c) amlodipine free base. Contour lines: blue, 400 mAU, green, 800 mAU, black, 1200 mAU and light blue, 1600 mAU. (II) Light microscopy photographs of the compacts containing (a) amlodipine besylate dihydrate, (b) amorphous amlodipine besylate and (c) amlodipine free base prior to and after imaging. The red arrows indicate crystal growth beyond the boundaries of the cylindrical compact. (d) Representative photo of compact within the channel flow cell showing crystal growth of amorphous amlodipine besylate upon dissolution imaging at static conditions. (III) Selected absorbance maps for the dissolution of sodium naproxenate in 0.01 M HCl containing 5.35×10^{-5} M thymol blue studied by dissolution imaging at 1.0 mL min^{-1} and 550 nm. Intense red color indicates high absorbance and the contours represent the *iso-absorbance/iso*-pH lines. Reprinted in modified form with permission from [97]. Copyright (2011) American Chemical Society. Reprinted from [144]. Copyright (2014) with permission from Elsevier.

hydrophobic surfaces. X-ray powder diffraction, offline Raman spectroscopy and dynamic vapour sorption (DVS) were used to confirm the solid-state forms of the drugs.

Østergaard and coworkers pioneered the use of UV imaging with *in-situ* Raman spectroscopy for characterising solvent-mediated solid form transitions during dissolution testing [136,137,138]. The dissolution behaviour of naproxen sodium and theophylline anhydrate and monohydrate with the simultaneous use of UV imaging and *in-situ* Raman spectroscopy, showed that decreases in their dissolution behaviour could be attributed to form changes where naproxen sodium and theophylline anhydrate both converted to their stable forms. The form conversion for theophylline anhydrate as detected by Raman spectroscopy occured within 5 min [136]. For the naproxen system, two intermediate forms were detected prior to formation of the stable form, which would readily have been overlooked by offline Raman spectroscopy. The use of *in-situ* Raman spectroscopy in combination with UV imaging seems to offer an interesting approach, which may be beneficial in preformulation and early drug phase development as it facilitates the understanding of basic dissolution behaviour and solvent-mediated solid form transitions.

Salt formation is an attractive option for improving solubility and bioavailability for ionisable drug candidates [145,146,147]. The solubility of twenty different Danirixin salts was determined with the hydrobromide salt giving the largest solubility improvement [148]. The effects of reduced gastric pH were investigated using simulated gastric fluid at pH 1.6, sodium phosphate, pH 3.0, and potassium citrate at pH 4.0. Dissolution studies showed improved dissolution rate for the hydrobromide salt as compared to the free base. This was most pronounced at pH 4.0, where a 6-fold increase was observed. The clinical study confirmed these findings with the hydrobromide salt having a greater bioavailability when compared to the free base [148]. A proof of concept setup was developed for mapping the local or microenvironmental pH change in relation to the dissolution of sodium naproxenate in 0.01 M and 0.10 M hydrochloric acid using the dissolution imaging a wavelength in the visible range and a pH indicator (thymol blue) [144] (Fig. 3 III). The dissolution of the sodium naproxenate in 0.01 M hydrochloric acid showed that sodium naproxenate could significantly change the microenvironment pH within the vicinity of the solid salt compact. The in-situ pH measurement is conceptually simple but requires some tailoring during method developments in terms of dye selection (pK_a, pH, concentration and wavelength). The dissolution performance of gemfibrozil and various salts with different alkyl chain lengths cyclopropylamine (CPROP), cyclobutylamine (CBUT), cyclopentylamine (CPENT) and cyclohexylamine (CHEX) were investigated showing all salts to provide increased IDRs relative to its free form (the free base). The results indicated that the longer alkyl chain length of the counter ion led to lower dissolution rates as compared to their shorter chain length counterparts [149].

Etherson et al. conducted an inter-laboratory investigation to assess variability in IDR determinations of drugs with low (tadalafil, bromocriptine mesylate), medium (carvedilol, indomethacin)

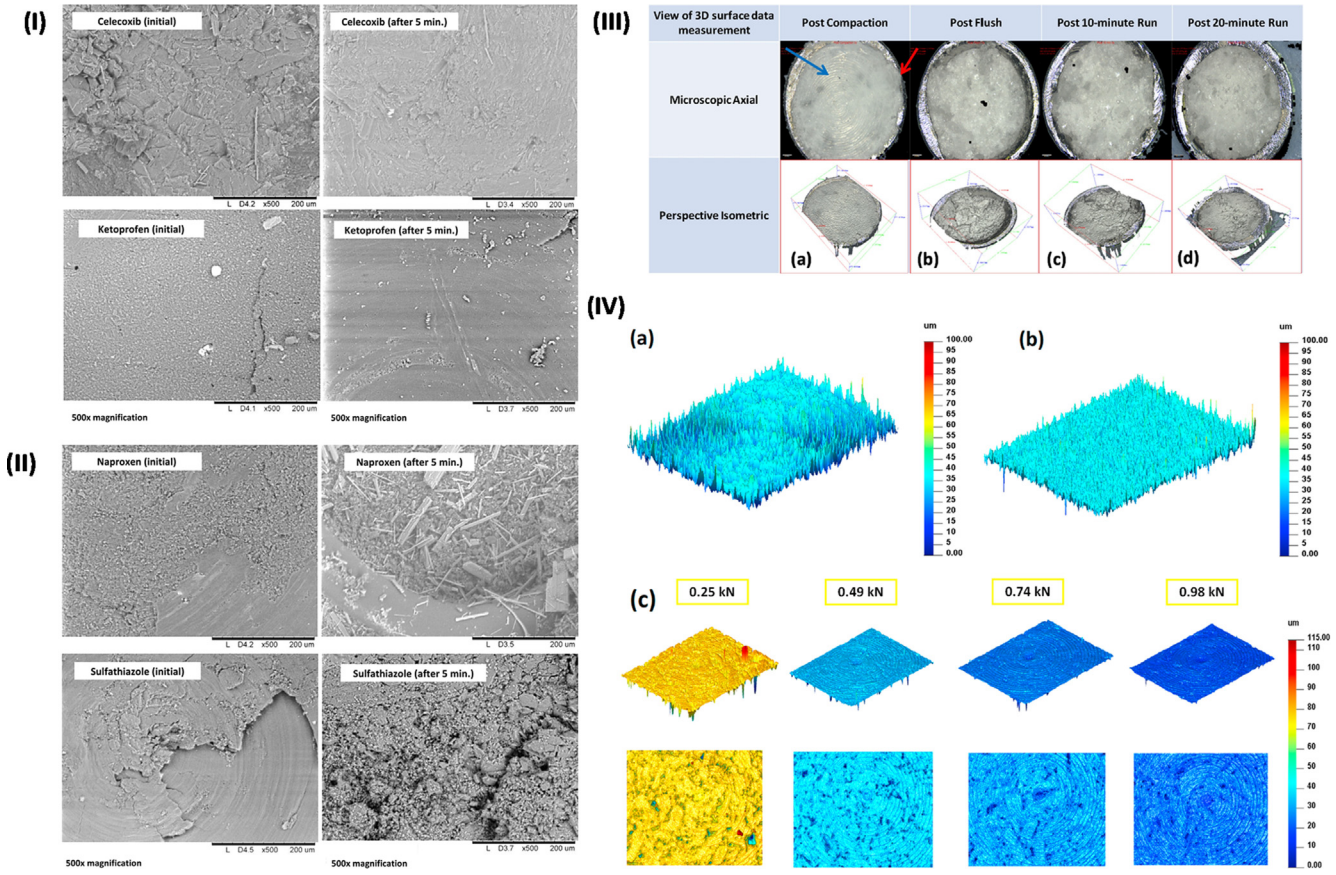

Fig. 4. Scanning electron microscopy images (×500 magnification) of (I) celecoxib and ketoprofen before and after 5 min of dissolution in biorelevant medium (FaSSIF) at 37 °C. (II) naproxen and sulfathiazole before and after 5 min of dissolution in biorelevant medium (FaSSIF) at 37 °C. (1II) Focus variation (Alicona™) 3D data set images of representative compacts of IBU (a) post compaction, (b) post flush, (c) after 10 min run on SDI, (d) after 20 min run on SDI. Note: diameter of sample holder in image is 2.5 mm (measured using a 150 mm digital calliper gauge from Draper Tools Ltd, UK). (IV) 3D images of the roughness of the original (a), and the manufactured plate insert surfaces (b), both used in the production compacts for IDR determinations. 3D images of the surfaces of IBU compacts at varying compressions of forces using the original press surface (c). Reprinted from [139], [140] and [143]. Copyright (2014, 2017, 2020) with permission from Elsevier.

and high (ibuprofen, valsartan) solubility using UV imaging [130]. The dissolution experiments were conducted in FaSSIF and blank FaSSIF at pH 6.5. These experiments were specifically conducted on the surface dissolution instrument (SDI) with Actipix™ Technology from Sirius Analytical, Forest Row, UK (now Pion Inc.). This study found that in general the rank order of mean IDRs reported across the six participating sites for each drug was similar to the solubility rank in both FaSSIF and blank FaSSIF. The variability in measurements, however, ranged from 33 % to 130 %, with the highest variability observed for the lowest solubility drugs. IDR data for indomethacin were selected for further analysis with the mean IDR data from a single operator compared to the site IDR data. A large reduction in the standard deviation could be achieved if a single operator was used for data analysis. Similar high variability related to IDR measurements was also found in another inter-laboratory study using the miniaturised dissolution instrument, the μDiss profiler [150]. These studies illustrate that, irrespective of standardised protocols for data collection the generation of repeatable dissolution data is far from trivial.

3.2.2. Biorelevant dissolution

Biorelevant dissolution media had little effect on the dissolution rate of furosemide [135]. It was observed that some samples had pronounced irregular upward shifts of the contour lines in UV absorbance maps, which may be an indication of dissolution followed by precipitation associated with solid form transformation or swelling of the solid material. *In-situ* Raman spectroscopy measurements were conducted and together with X-ray diffraction confirmed that this was not due to solvent mediated solid form transformation (showing the difficulty associated with inferring form changes from dissolution rates and visual characteristics). These observations warranted further studies of the dissolution behaviour of amorphous furosemide sodium salt and amorphous furosemide (acidic neutral species) in simulated bio-relevant intestinal medium at pH 6.5 [151] along with its corresponding crystalline forms [152]. *In-situ* Raman spectroscopy measurements were employed to gain an insight into solvent mediated form changes. This study also included IDR determinations conducted on a μ-Diss profiler for comparison purposes. IDR determinations for the four furosemide samples showed that the two salt forms had a higher dissolution rate when compared to the acid forms, with the highest dissolution rate observed for the amorphous salt form. Fast conversion of the two amorphous forms to trihydrate forms was shown by both a decrease in dissolution rate and changes in Raman spectra.

Niederquell and Kuentz determined the IDR of celecoxib, ketoprofen, naproxen, and sulfathiazole in simulated gastric biorelevant media at pH 6.5 [143]. High and variable initial drug dissolution rates observed by the UV imaging dissolution, which was followed by decreasing dissolution rates with time. This was attributed to sample heterogeneity. High and variable initial dissolution rates have also been observed in other studies [97,98,135]. Niederquell and Kuentz modelled the heterogeneity effects using double logarithmic plots of the dissolution rate versus time and fractal-like dissolution behaviour as the profiles adhered to a power law relation. Although the initial phase was dominated by

effects of surface heterogeneity, the ensuing phase could be viewed as a pseudo-equilibrium meaning an intrinsic drug dissolution rate could be inferred from this range [143]. The sample heterogeneity was confirmed using SEM (Fig. 4 I and II). This study depicted how heterogeneity-related effects could affect dissolution experiments on small-scale dissolution systems. Other authors have used similar models to evaluate solvent-mediated changes of APIs; in solid dispersions systems, dosage forms as well as surfaces of nanocrystals [153,154,155,156 157]. Sample surface heterogeneity has been characterised quantitatively to provide information on the surfaces for compacts prior and post UV dissolution using focus variation microscopy (FVM) [139,140] (Fig. 4 III and IV). Focus variation microscopy was employed with the view of establishing a relationship between drug compact surface properties and dissolution performance [139]. The surface parameter of *Sdr*, which gives an estimation of changes in surface area was of particular interest and showed a general decrease of the surface area by the dissolution process (this however was a decrease from the "post flush" to the end of the dissolution process). The IDR also decreased as the experiment continued, with higher IDR values reported during the first 10 min as opposed to IDR values reported after 20 min as observed previously [143]. Such studies show that drug compact surface properties may impact IDR determination. An investigation into the influence of compaction force on three different API (ibuprofen, ketoprofen and paracetamol) compacts compressed against different surfaces showed that generally, higher pressures resulted in a flatter, smoother compacts as reported by decreases in the *Sdr* parameter. When compacts were made on a manufactured relatively smoother surface for both the ibuprofen and paracetamol, their compacts however experienced increases in the *Sdr* parameter indicating a larger surface area to be associated to the compacts. This suggested that the ability of the drugs to form smoother drug compacts may be API dependent [140]. The change in surface properties however, did not seem to significantly affect the dissolution rate, suggesting the solubility of the drug to be a predominant factor in the dissolution process [140].

3.2.3. Co-amorphous systems

Co-amorphous systems present an attractive approach for stabilising amorphous compounds which can be prone to

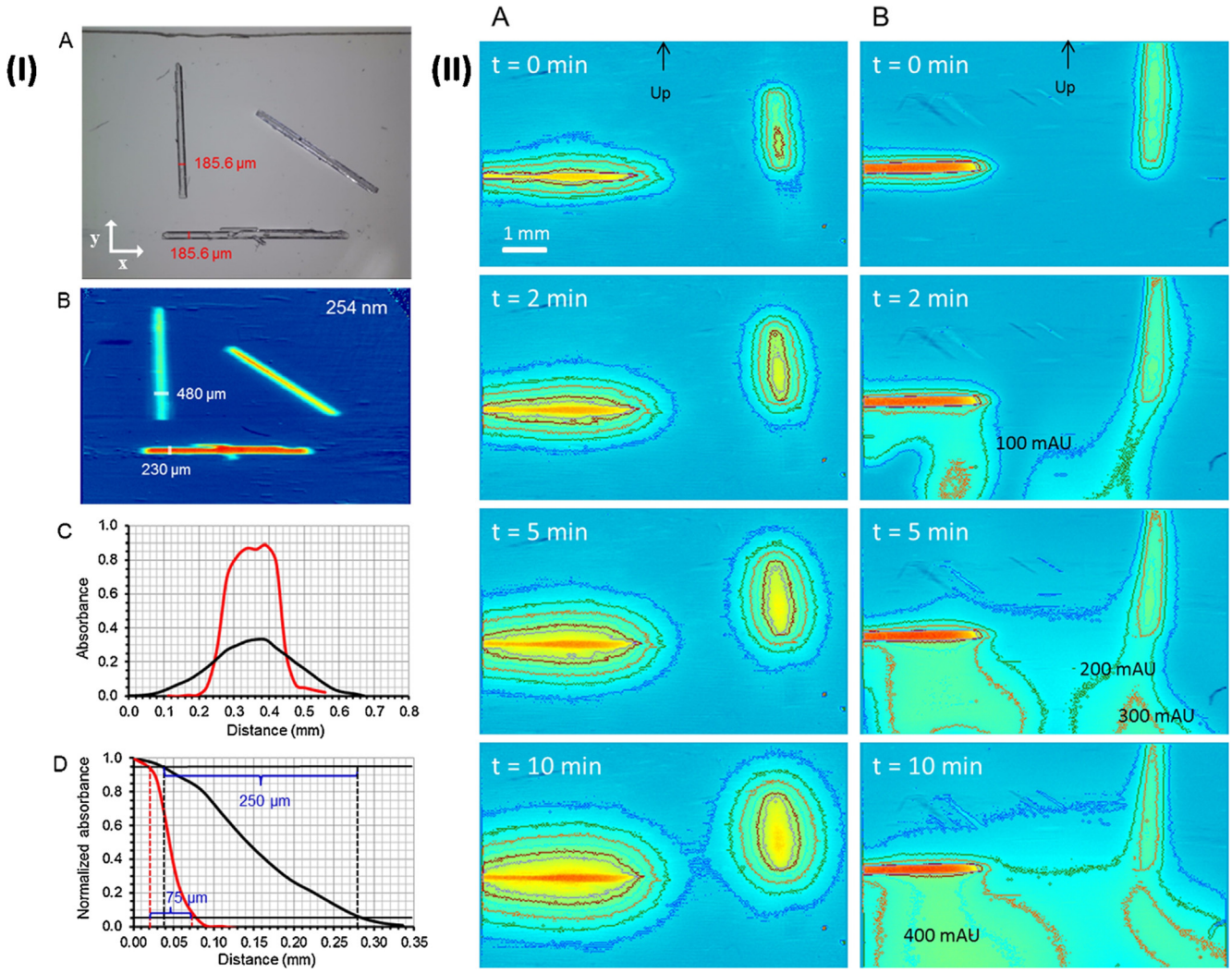

Fig. 5. (I) (A) Microscope photograph (the image is 8.3 × 6.4 mm^2) and (B) absorbance maps of the lidocaine crystals arranged in a quartz cell obtained by the Sirius SDI imaging system with pixels binned 4 × 4 at 254 nm. The image is 10.4 × 4.6 mm^2. (C) Absorbance – y-distance profile of the lidocaine crystal placed in the x-direction (▬) and absorbance – x-distance profile for crystal placed in the y-direction (▬) for determining the width of the crystals from the absorbance maps and (D) normalized absorbance – distance profile of one side of a lidocaine crystal placed in the x-direction (▬) and y-direction (▬) for estimating the resolution of the Sirius SDI imaging system. . (II) Time-dependent absorbance contour maps of the dissolution of lidocaine crystals in (A) 0.5% (w/v) agarose gel, pH 7.4 and (B) 0.067 M phosphate buffered solution, pH 7.4. The dissolution was performed in quartz cells with 1 mm light path using the Sirius SDI UV imaging system with the pixels binned 4 × 4 at 254 nm and the sensor head placed in the upright position. Reprinted from [126]. Copyright (2016) with permission from Elsevier.

recrystallization, especially when stored in humid conditions or above their glass transition temperature [107,158,159]. These systems as compared with their respective crystalline forms have no long-range crystallographic order and higher internal energy [160,161,162]. Recently, UV dissolution imaging with in-situ Raman spectroscopy was used to investigate the solvent-mediated transformation in the co-amorphous system composed from naproxen and naproxen sodium during dissolution [138]. Solid-state analysis using XRD, DSC and FTIR showed that the 1:1 naproxen and naproxen sodium salt co-amorphous system was stable for 2 months at 40 °C. For comparison, dissolution studies were also conducted on a physical mixture, sodium naproxen and naproxen (free acid). UV imaging showed that the dissolution rate of the co-amorphous system was between that of the crystalline free acid and the sodium salt. Although a co-amorphous was successful produced, it somewhat surprisingly did not lead to any improvement in dissolution rate over the pure sodium salt. *In-situ* Raman spectroscopy measurements revealed initial phase separation of the co-amorphous form to naproxen free acid and sodium naproxen followed by disproportionation of the sodium salt and crystallization to free acid naproxen. This to date has been the only study of its kind, however, UV imaging with simultaneous *in-situ* Raman spectroscopy may provide further detailed insights into these systems.

3.2.4. Single crystal and nanocrystal dissolution

An early UV imaging study visualized the dissolution of lidocaine from a single crystal in stagnant phosphate buffer, pH 7.4 [126] (Fig. 5). Imaging at 254 nm revealed dissolved lidocaine falling towards the bottom of the quartz cell due to natural convection caused by the local density gradients formed from dissolution of the highly soluble lidocaine. Quantitative estimates of the amount of lidocaine dissolved from the crystal were obtained from the UV images. The natural convection can be efficiently suppressed by imbedding the crystal in a gel matrix; symmetrical diffusion patterns around similar lidocaine crystals placed in agarose gels have been reported [99]. Single crystal dissolution and, in particular, face specific dissolution of single crystals may provide fundamental knowledge regarding the mechanism of crystalline API dissolution. Apparently, it has proved difficult to progress from the initial studies cited above to face specific dissolution measurements using UV imaging. Among the challenges encountered are crystal size, resolution and difficulty to resolve crystal faces from dissolved compound. At present, other approaches seem more promising as relates to face specific dissolution [163,164,165,166,167]. The key interest from pursuing UV/Vis imaging in this area should relate to the ability to attain information about both the dissolved drug (UV wavelength) and the solid (Visible wavelength) in a single measurement.

One of the techniques to improve the bioavailability of poorly soluble drugs is the use of the nanocrystal approach [168,169]. UV imaging alongside a traditional flow-through dissolution method showed dissolution improvements of indomethacin nanocrystals prepared using a top-down wet milling technique with poloxamer F68, poloxamer F127 and polysorbate 80 as stabilizers, as compared to unmilled indomethacin and their physical mixtures [170]. The initial UV and Vis imaging, however, showed significant absorbance increases during the flow-through dissolution at 265 nm and 550 nm. This was explained by nanocrystals liberating from the surface of the compact into the dissolution medium scattering and absorbing light at 550 nm. A hydrogel matrix was used in the suppression of these particles "escaping" from the compact surface. This resulted in the nano-crystal compacts having a significantly higher dissolution rate as compared to unmilled indomethacin (five times the solubility in the immediate vicinity of the nanocrystal compact, which may be due to supersaturation). It is important to note that the poloxamer F68 and F127 might also have local solubilising effects on indomethacin.

Polymeric strip-films constitute a versatile drug delivery platform that has recently received significant attention and are capable of incorporating active substances in thin polymer matrices that allow its delivery upon oral administration [171,172,173]. The feasibility of using a drug-loaded hydrophilic (HPMC) polymeric layer sandwiched between two hydrophobic poly-ε-caprolactone (PCL) layers for improving film drug load whilst achieving sustained release of fenofibrate was investigated [174]. Thinner films followed Fickian diffusion, and thicker films followed non-Fickian anomalous diffusion as modelled from drug release rates obtained using the USP IV flow-through cell and a UV dissolution imaging system. Changing the thickness of the middle layer allowed manipulation of drug load without the need for altering the formulation composition. Fenofibrate nanocrystals were incorporated into oral strip-films of variable thickness and compared to a marketed formulation (Tricor) [175]. *In-vivo* pharmacokinetic properties of the different thickness oral films were also investigated using rabbits. The bioavailability of the nanocrystal films was improved by a factor of 1.4 to 1.8 fold as compared to the marketed formulation. Solid-state analysis suggested that fenofibrate nanocrystals were successfully incorporated into the oral strip-films and the crystalline state remained unchanged and stable. UV dissolution imaging results qualitatively showed the swelling associated with the films as well as visualisation of the drug release. Quantitatively, the UV dissolution imaging showed that the fastest dissolution occurred using the thinnest film and was comparable to the dissolution studies using the USP-IV dissolution apparatus.

3.3. Drug-excipient compatibility

Although limited structural information can be obtained from UV–Vis spectra as compared to other chemical imaging techniques, UV dissolution imaging may allow for visualisation of dissolution phenomenon such as drug-polymer interactions, differentiation between polymer grades, viscosity effects of formulated products and ranking of salts. Here the applications of UV imaging involving excipients is discussed.

UV imaging was used to visualise the swelling behaviour of compacted 15 cP and 50 cP viscosity grades of hydroxypropyl methylcellulose (HPMC or hypromellose), a hydrophilic polymer widely used to the control API release in oral formulations under flow as well as under stagnant conditions [176] (Fig. 6 I). UV imaging at 214 nm was able to detect polymer entanglement, swelling and eventual gel formation instrumental in controlling drug release. The experimental set-up provided sufficient sensitivity for differentiating between the two viscosity grades of HPMC, showing a faster and more pronounced swelling with HPMC 50 cP compared to 15 cP. The swelling behaviour of 3D printed cellulosic tablets matrices for disintegration visualized by UV imaging revealed that cellulose matrix swelling was between 0.2 and 0.4 mm. The spacing gaps around the 3D printed cellulosic tablets matrices would therefore be ineffective once exposed to dissolution medium as they would be closed off as the polymer swelled. Results from the USP apparatus II testing supported the swelling closed gap hypothesis observed from the UV dissolution imaging, as the 3D tablets with the narrowest gaps of 0.2 mm showed the slowest drug release and longest time to fragment [177].

Amorphous solid dispersions (ASDs) constitute a widely used approach for improving the solubility and bioavailability of poorly soluble APIs. Here, the crystalline drug is amorphisized or molecularly dispersed within a synthetic or naturally water-soluble polymer such as polyethylene glycol (PEG), soluplus,

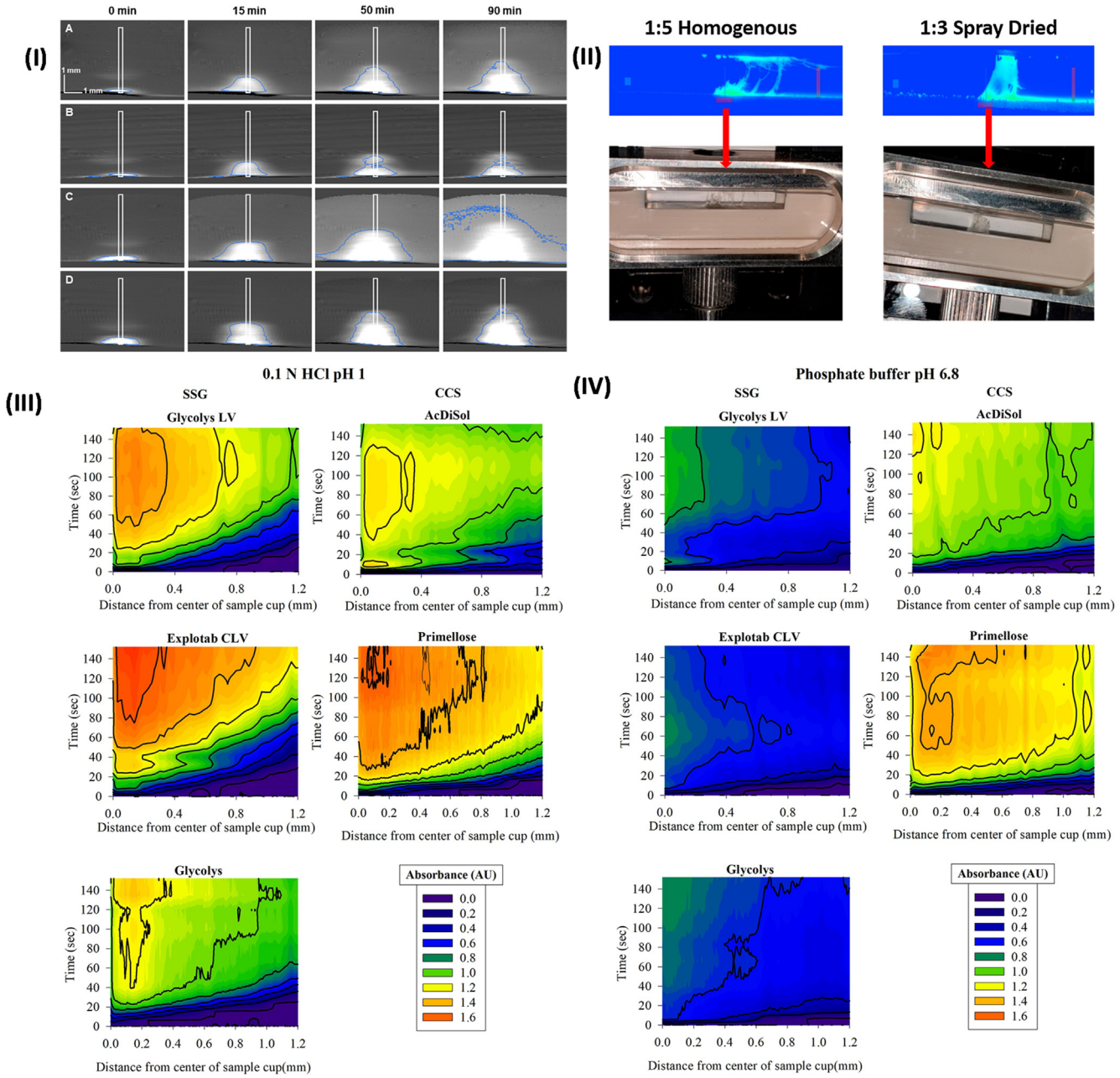

Fig. 6. (I) Images of HPMC 15 cP in stagnant medium (A) and flow of 0.5 mL/min (B), and HPMC 50 cP in stagnant PBS (C) and in presence of flow (D) at time points of 0, 15, 50 and 90 min. The white colour represents absorbance caused by the polymer, the contour line corresponds to an absorbance threshold of gel point, i.e. 3.2% (w/w) for HPMC 15 cP, and 2.3% (w/w) for 50 cP, and the rectangle designate the area, in which the analysis was performed. (II) Images captured of the web-like phenomenon within the IDR flow through cell taking place in the UV experiments. Absorbance values (Abs) of the studied superdisintegrant types and brands as a function of distance from the centre of the sample cup (mm) in (III) 0.1 N HCl pH 1 (SDI1, 0 mL/min, 37 °C, 254 nm) presented up to 2.5 min. (IV) in phosphate buffer pH 6.8 (SDI1, 0 mL/min, 37 °C, 254 nm) up to 2.5 min. Reprinted from [176], [105] and [189]. Copyright (2012, 2019 and 2020) with permission from Elsevier.

polyvinylpyrrolidone (PVP) or hydroxypropyl methylcellulose (HPMC) [178,179,180,181,182,183,184 185,186,187]. ASDs of nilotinib were prepared with the polymer hydroxypropyl methylcellulose phthalate (HP55) (as well as with HPMC). The produced amorphous nanodispersions were investigated using UV dissolution imaging with in-situ Raman spectroscopy [137]. Two nilotinib nanoparticle dispersions of 20 % and 40 % drug load and physical mixtures were investigated while invoking a pH change from pH 2.2 to 6.4 during the UV dissolution imaging. Extensive physicochemical testing on the dispersions produced showed that the nilotinib drug load had little effect on the physical state of the API but had significant effects on the dissolution properties, with the higher drug load showing increased dissolution rate when compared to the ASDs with 20 % drug load, the pure drug and both physical mixes. This enhancement was attributed to the stabilising effects of hydrophobic and H-bond interactions, which, particularly at higher drug loads prevented the formation of crystalline nilotinib. Dissolution experiments were also conducted using USP apparatus II and it was observed that a marked decrease in dissolution rate at 30 min was observed when the pH change occurred. This was, however, less profound in the UV imaging testing [137]. Gautshci et al. investigated whether increases with respect to IDR could be achieved by solid dispersions prepared by the addition of either mono or diacyl lecithin phospholipid to a series of poorly

soluble drugs (BCS class II and IV) [188]. Phospholipid:drug 1:1 M ratios were investigated. The ability of the drug substances to form solid dispersions with the phospholipids were related to the APÍs physical chemical parameters such as the frontier orbital energy, enthalpy of fusion, and log *P*. UV imaging results showed an improvement in IDR when using the monoacyl lecithin phospholipid as compared to the diacyl lecithin phospholipid and pure drug.

Indomethacin-Soluplus ASDs prepared by spray drying, freeze drying and using a homogenising-freeze drying technique were also assessed using UV dissolution imaging [105]. It was observed that the samples with the lower polymer content had improved drug release rates as revealed by flow-through UV dissolution imaging. The higher ratios of Soluplus resulted in the formation of a web-like pattern of polymer swelling within the cell (Fig. 6 II). These formed web-like strands, which attached to the top of the flow cell and may have resulted in the decrease in drug liberation from the compacts.

The UV dissolution imaging effects of pure or amorphous forms of cefuroxime axetil and itraconazole using FaSSGF and FaSSIF-V1 biorelevant dissolution media and simulated gastric fluid without pepsin (SGF) and fasted state simulated intestinal fluid without pancreatin (SIF) were investigated [190]. The drug formulations Zinnat tablets (cefuroxime axetil) and Sporanox capsules (itraconazole) were used to provide the amorphous forms of the drug substances and were crushed and made into a compact in preparation for UV imaging testing. This, however, proved challenging for Zinnat as the presence of a superdisintegrant resulted in a physical blockage of light in the flow cell. The Sporanox formulation contained HPMC, which swelled and thereby had an effect on drug release from the HPMC polymer matrix. For the compacts under investigation, the higher flow rates resulted in an increased drug release from the compact surfaces. The pure drug, itraconazole compacts exhibited slightly increased drug release from the surface of its compacts over the amorphous form in the Sporanox formulation, however the excipients in this formulation may have affected these results. Hiew et al. investigated the impact of excipient shielding on release of acetylsalicylic acid [191]. A number of compacts were produced, containing different ratios of drug and the excipient microcrystalline cellulose (MCC). Offline Raman spectroscopy was used to establish the distribution of MCC on the surface of each drug-excipient compact. Two different acetylsalicylic acid particle size fractions were investigated. This resulted in IDRs, which were broadly similar and could only be statically distinguished at lower acetylsalicylic acid to MCC ratios. A flow rate of 0.1 mL min^{-1} was deemed preferable as it achieved IDRs with the lowest standard deviation. This study showed that MCC at higher concentrations (75 % and over), resulted in initial suppression of acetylsalicylic acid dissolution and lower maximum IDR values [191]. Madelung et al. utilised UV imaging to investigate the dissolution enhancement of the incorporation of sodium dodecyl sulfate (SDS) into griseofulvin compacts [192]. This was achieved by production of a griseofulvin-SDS solid dispersion disc or the addition of SDS into the dissolution media. SEM-EDX prior to dissolution showed heterogeneity with respect to the distribution of griseofulvin and SDS. The initial high dissolution rate was attributed to the loose particles on the surface of the compacts as revealed by SEM analysis. Results showed that higher SDS concentrations either in the buffer or incorporated into the disc showed the largest improvement in griseofulvin dissolution rate [192]. A key excipient used in immediate release formulations are superdisintegrants as they promote fast tablet disintegration. Zarmpi et al. utilised UV imaging to investigate the impact of two superdisintegrants (Fig. 6 III and IV) on the dissolution of paracetamol and carbamazepine. The viscosity of sodium starch glycolate (SSG) was varied by applying three brands of the superdisintegrant (Explotab - low viscosity, Glycolys - low viscosity and Glycolys - high viscosity). Particle size distribution was also investigated using two brands of croscarmellose sodium (CCS), (AcDiSol - small particle size and Primellose - large particle size). All drug compacts containing superdisintegrants resulted in a higher dissolution rate when compared to the pure drug compact. This was attributed to the enhanced wetting of the compacts or compact disintegration. Pronounced dissolution rate enhancement was achieved by the low viscosity SSG and small particle size CCS and was more effective for the higher solubility drug paracetamol, as compared to carbamazepine. Paracetamol showed a faster dissolution in neutral solution than at acidic pH. This was largely attributed to increased excipient hydration. The opposite was true for the poorly soluble drug carbamazepine. This was attributed to the swelling of excipient on the surface of compact, which impeded drug release [189].

4. Whole dose imaging

The introduction of the USP type IV-like whole dose cell in dissolution imaging (SDI2) facilitated studies on tablets and capsules not possible with the early smaller UV imaging instrumentation. A typical image generated by the UV imaging dissolution instrument for a whole dosage form is depicted in Fig. 7. The dissolution of carbamazepine is apparent as the increase in absorbance at 280 nm. The carbamazepine dissolved from the tablet is carried with the flow exiting the flow cell at the top side. Quantitative information may be extracted from the images captured. Measurement of the drug concentration above the tablet is conducted using the so-called drug measurement zone, and subsequently used for calculation of the dissolution rate (Fig. 7). The apparent carbamazepine concentration distribution in the cell reveals turbulent flow conditions.

The first mentioning of whole dose UV dissolution imaging showed the simultaneous release of metformin from (255 nm) and the swelling (520 nm) of a commercial Glucophage SR tablet [16]. In addition to the larger imaging area allowing the assessment of larger dosage forms, the dual wavelength imaging capability of the recent UV/Vis imaging instrumentation importantly provided the possibility to separate absorbance due to released drug substance from the signal due to the formulation or excipi-

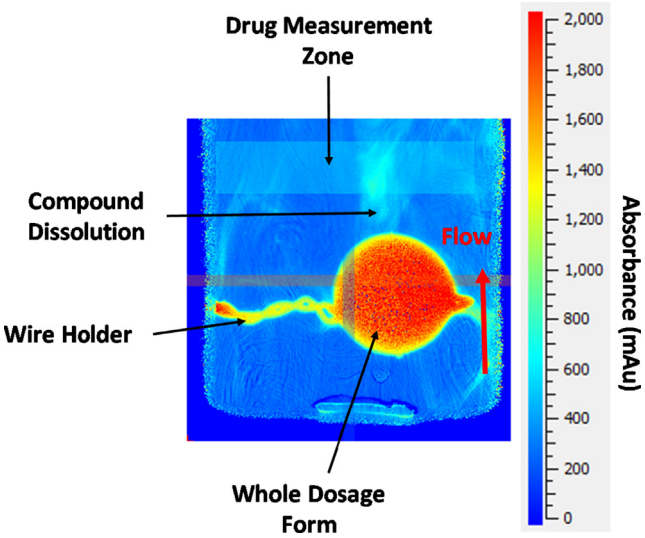

Fig. 7. Image from the analysis software of the UV dissolution imaging instrument (Pion SDI2). Image shows the dissolution of carbamazepine from a tablet in 1 % SDS solution at a flow rate of 8.2 mL/min at 37 °C. Detection at 280 nm. (Asare-Addo. Unpublished data).

ents. This feature has also improved the possibility of relating drug dissolution to physical changes in the formulation or delivery system [16].

The oral drug delivery route still remains the route of choice over other delivery systems [195,196]. By formulating a drug to include a hydrophilic polymer matrix, modification of the kinetics of drug release from orally administered solid dosage forms can be pursued. Hydrophilic swellable polymers often used include HPMC, poly(ethylene oxide) and hydroxypropylcellulose (HPC) [27]. Upon exposure to water or biological fluids, the hydrophilic

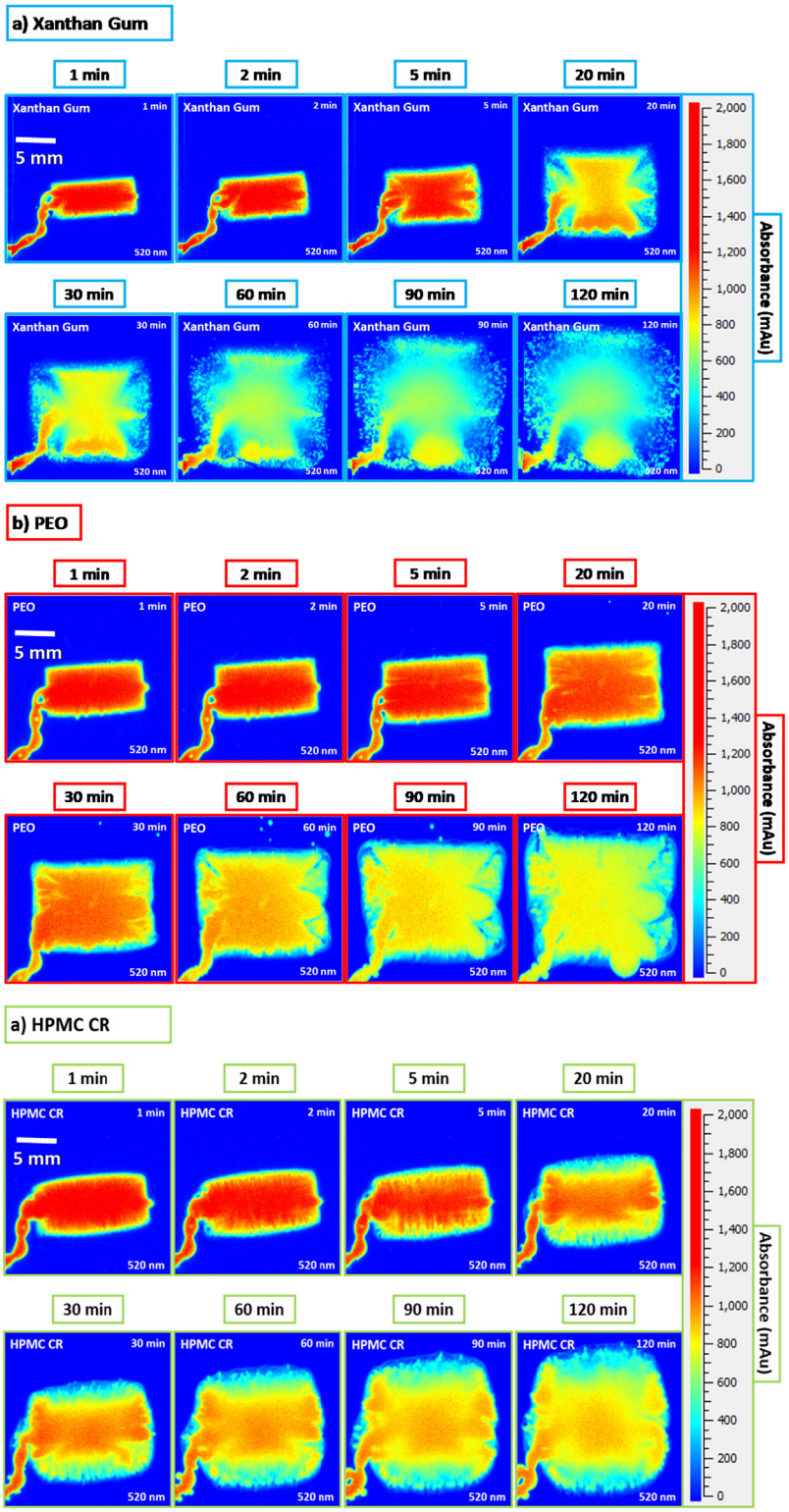

Fig. 8. Optical images obtained from the dissolution imaging system at the 520 nm wavelength: (**a**) XG, (**b**) PEO, and (**c**) HPMC CR. Note: Images are taken from the 2 h experiment at time intervals of 1, 2, 5, 20, 30, 60, 90 and 120 min. XG is xanthan gum, PEO is polyethylene oxide, and HPMC CR is hypromellose K100M CR grade. Reprinted from [201]. MDPI (Open Access).

polymer becomes hydrated, swells and forms a gel layer around an initially dry core [184,195,196,197,198]. This gel layer hydration process is dynamic. The inward migration of fluid or ingress of fluid means that the gel layer grows over time. The thickness of the gel layer can delay the diffusion of an incorporated drug [195,196]. To this end, Ward et al. [106] developed a method to allow the measurement of the developed gel layer from hydrophilic matrices. Tablet measurement zones, absorbance thresholds and medium flow rates were investigated to determine the appropriate parameters required to facilitate repeatable measurements of swelling in hydrophilic matrices using the Vis imaging capability of the dissolution instrument. Using the CR and DC grade of hypromellose, the authors reported similar swelling for both grades despite the difference in morphology and differences in porosity as a result [106]. The images produced, showed denser gels to form for the CR grade potentially as a result of the porosity differences, which may be missed by compendial methods. Li et al. [107] investigated the effect of Methocel K15M, K100M and microcrystalline cellulose (MCC) effects on theophylline release. Simultaneous imaging of drug release at 255 nm and swelling at 520 nm showed the distinctly different behaviour of the Methocel polymers relative to the MCC matrix demonstrating the potential of the imaging system to characterise excipients as well as potential drug-excipient interactions. The early onset of the gel layer in hydrophilic matrices is of importance especially for the controlled release of soluble drugs to ensure dose-dumping does not occur [199,200].

The *Smr2* parameter from the focus variation microscope, which reflects the ratio of the area of the material (compact) at the intersection line, which separates the dales from the core surface to the evaluation area was used as a proof of concept predictive tool in determining wetting and initial hydration from a natural (xanthan gum, XG), semi-synthetic (hypromellose, HPMC) and synthetic (polyethylene oxide, PEO) polymer using the whole dose cell. *Smr2* can also be used to calculate the percentage of 'valleys' that will retain lubrication and was applied to determine the percentage of the compact surface available for wetting during the initial hydration process. The porosity of the compacts produced were in the order XG > HPMC > PEO. From the porosity perspective, it was therefore expected for the initial wetting and gel layer to be in the self-same way. The *Smr2* parameter, however, from the FVM analysis suggested the tablet surfaces able to retain more lubrication and therefore wet quicker to be in the order of XG > PEO > HPMC. The whole dose imaging of the wetting and early gel layer formation concurred with the *Smr2* prediction confirming it was possible to predict initial wetting therefore suggesting differences in porosity was not a major indicator for water ingress [201] (Fig. 8).

The rate of drug release from matrices can be influenced by formulation variables as well as by the composition of the surrounding medium it is exposed to after ingestion, such as pH, enzymes, electrolytes and surfactants [202,203,204]. The liquisolid technique has been used as a means for either slowing down (high solubility APIs) or increasing (poorly soluble APIs) drug release [205]. Propranolol hydrochloride release from liquisolid compacts of sesamum gum polysaccharide was successfully imaged qualitatively and quantitatively using the UV dissolution imaging [104].

The pharmaceutical industry utilizes film coatings for various reasons which includes but not limited to aesthetics, trade marking, taste masking of bitter APIs, product stability, drug release manipulation through retardation and providing resistance to the harsh conditions experienced in the stomach [206]. Gaunø, et al. utilised UV dissolution imaging to investigate the release of 5-aminosalicylic acid from single extrudates, with an ethyl cellulose layer coating into a 0.5 % (w/v) agarose hydrogel [207]. The effect of varying coating thicknesses on drug dissolution was investigated. The thickness of ethyl cellulose layer coating was determined by percentage weight gain, four different variations were used (0.5 %, 1.0 %, 1.5 % and 2.0 % weight gain). Dissolution testing was also performed using a conventional paddle dissolution system. The same rank order of dissolution performance for different coated extrudes was reported in each dissolution method, with the highest dissolution rate reported in the thinnest coated extrude and the lowest from the thickest coat. Studies were conducted to establish the impact on damages to the extrudate coating, this showed a faster dissolution rate from the damaged extrudes thereby exhibiting the technique for potential trouble shooting. Alqahtani et al. [208] investigated the use of low quantities of functional additives to control drug release from hot-melt extruded solid dispersions of carbamazepine (extrudates). The UV imaging aspects corroborated with the conventional dissolution studies (basket method). The disintegration process of the surface of the extrudates containing gelucire was also visualised which was missed by the conventional basket method.

Zarmpi et al. used a QbD approach to investigate the effect of superdisintegrants, viscosity of binders, particle size and lubricants on the release of a soluble (paracetamol) and poorly-soluble (car-

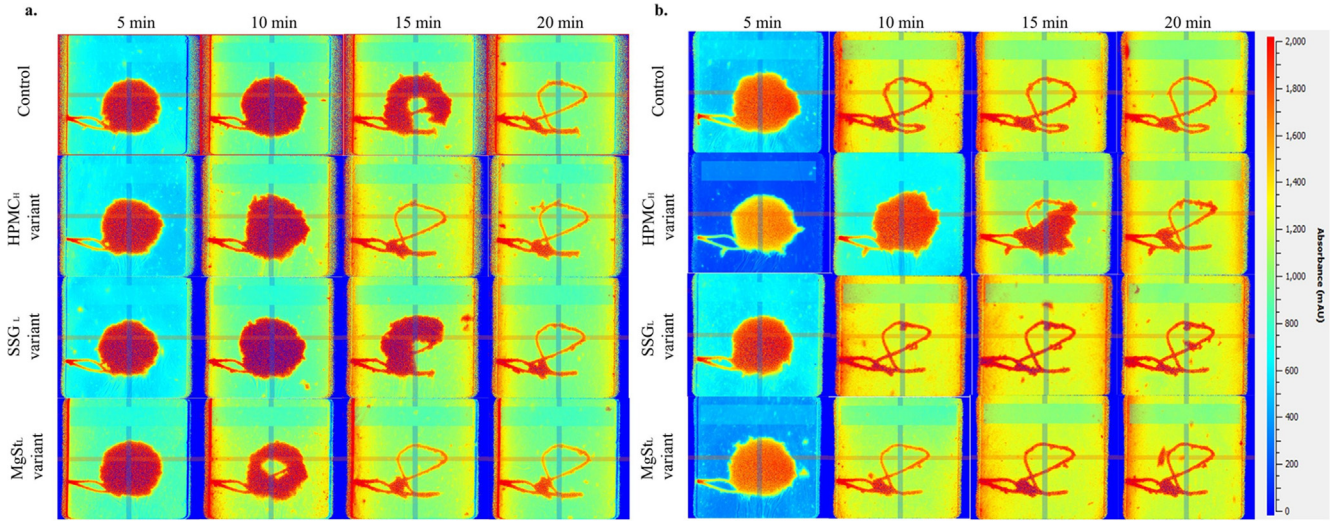

Fig. 9. Real-time surface dissolution UV images for a. PRC and b. CBZ tablets in 0.1 N HCl pH 1. Reprinted from [209]. Copyright (2020) with permission from Elsevier.

bamazepine) model compound from compacts made using blends of API and varying concentrations of superdisintegrants [209]. It was observed from the UV dissolution imaging process that for the highly soluble drug, a high viscosity binder and smaller particle size lubricant caused a quicker disintegration process whereas for the poorly soluble drug, a slower disintegration was observed with an increase in the viscosity of the binder as compared to the control compacts of pure API (Fig. 9). The UV imaging thus provided a visualisation of the disintegration and dissolution process.

The whole dose dissolution imaging has been used in the evaluation of several salt forms of the carboxylic acid gemfibrozil [194]. The formulated salts exhibited increased dissolution over the parent drug gemfibrozil and correlated with the rank order using the IDR compact cell as reported earlier. The whole dose dissolution imaging used in the assessment of the release of indomethacin from ASDs with Soluplus showed that the solid dispersions regardless of the ratio of Soluplus or preparation method had an increased dissolution rate as compared to its parent drug (indomethacin only). Here, a different outcome to that of the rank order produced by UV disolution imaging compact cell was observed [105]. UV and Vis images depicted the tip of a capsule opening for the liberation of the indomethacin drug. UV imaging has also been used to provide insights into the dissolution behaviour of 3D printed formulations. Arafat et al. investigated sodium warfarin release from 3D printed dosage forms at a wavelength of 255 nm [210]. The visible wavelength of 520 nm was used to visualise the erosion of the methacrylate used in the 3D printing of the matrix. The ability of the dissolution method to simultaneously monitor the sodium warfarin release and the erosion of the methacrylate showed that the bulk of the drug release to occurred via a diffusion process prior to polymer erosion at a rate of 16.4 and 15.2 μm/min in the horizontal and vertical planes, respectively.

5. *In vitro* release testing - non-oral routes of drug delivery

Most studies involving UV imaging have concerned the assessment of dissolution behavior in the context of oral drug delivery, e.g., intrinsic or tablet dissolution. However, one of the very first UV imaging applications was the release of nicotine from transdermal patch samples [211]. The ability to image concentration gradients and drug transport is of potential value for elucidating release processes relating to most routes of administration and formulation approaches. In general, UV imaging may be suitable for assessment of drug release when the API possesses a chromophore and the release medium or matrix is sufficiently transparent at the relevant wavelength(s). The physical form and geometry (size) of delivery vehicle, complexity of the formulation as well as the release matrix are additional parameters that should be considered in relation to image area and resolution prior to embarking on UV imaging-based release testing. In this section, the application of UV imaging for characterization of parenterals is covered; special applications directed at physicochemical characterization of the active substance by UV imaging are discussed in Section 6.

5.1. Injectables

Similar to *in-vitro* dissolution testing for oral products, *in vitro* release or drug release testing is a key tool for characterization of injectable sustained release formulations. *In vitro* release testing for injectable parenterals is of importance throughout formulation development and in quality control. The use of the compendial methods, developed mainly for oral drugs or transdermals, has been endorsed and utilized with variable degrees of success [212,213]. Relative to oral drug delivery this field is less well developed; pharmacopeieal reference methods remain to be established

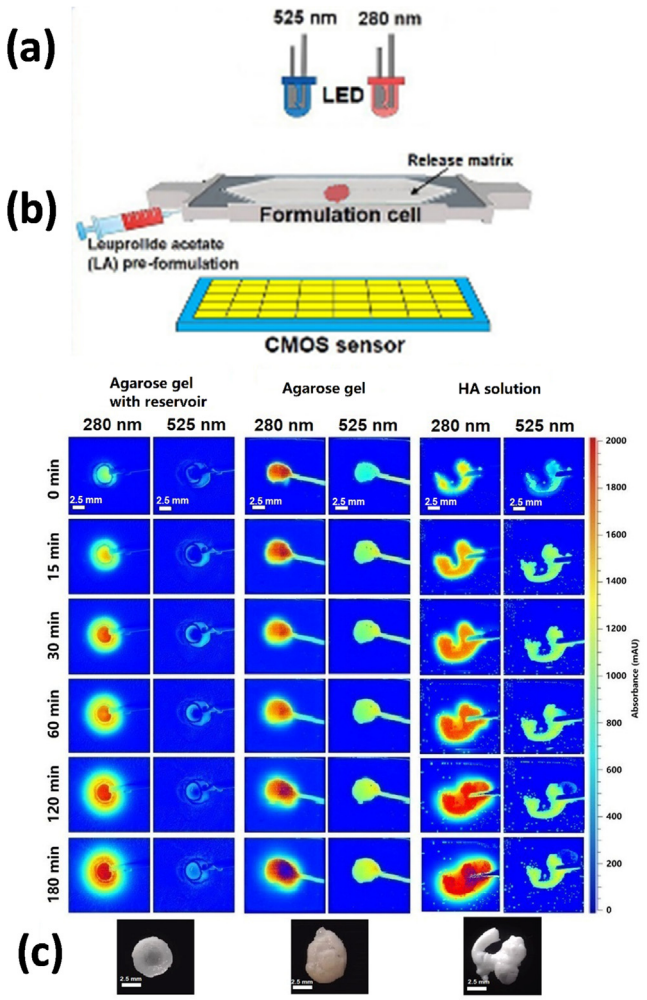

Fig. 10. Schematic representation of the D200 UV–Vis imaging system for monitoring release of leuprolide acetate from in situ forming PLGA implants (A), representative absorbance maps obtained by UV imaging at 280 nm and vis imaging at 525 nm in 0.5% (w/v) agarose gel and 10 mg/mL HA solution upon injection of the PLGA/NMP pre-formulation containing 3% (w/w) LA (B), and photographs of the corresponding implants removed from the release medium after the experiments (C). Reprinted in modified form with permission from [102]. Copyright 2020 American Chemical Society.

for injectables [212,214]. A standardized *in vitro* release testing method for injectables is recognized as highly desirable but also a difficult to reach objective given the diversity and complexity of injectable formulations [213,214]. Typically, *in vitro* release tests for injectables are classified as sample and separate, dialysis membrane or continuous flow methods. A coverage of the general features of the three types of methods and the variability among the classes can be found in several reviews, e.g., [215,216,217,218,219].

Somewhat surprisingly, given the commercially promoted flow cells for dissolution testing, UV imaging continuous flow methods for injectables have not yet been reported. Membrane-based methods in connection with UV imaging also appears not to have been explored in relation to injectables, albeit to permeability studies [220]. The use of UV imaging in relation to injectables has been connected to the use of gel matrixes as the receiver medium [221,222,223,224,102,225]. A distinct and useful feature of UV imaging for *in vitro* release testing is the possibility of performing the release studies in a non-intrusive manner and without the need for compound labeling, thus, perturbation of the system or release process may be avoided. On this basis, it may be argued that the UV

imaging methods do not belong to the group of sample and separate methods either. However, the ability to separate the absorbance signal due to the released drug from the absorbance of the formulation and matrix is required in UV imaging-based release studies.

Various hydrogel constructs have attracted interest as soft tissue mimicks in relation to drug release testing [226,227,228,229,230,231,232,233,234,235]. In relation to UV imaging studies, primarily agarose gels have been applied due to their robustness and transparency [236]. Ye et al. studied piroxicam release from medium chain triglyceride (MCT) into either 0.5 % (w/v) agarose or 25 % (w/v) Pluronic F127-based hydrogels serving as simple subcutaneous tissue models [221]. Vegetable oils, like MCT, serve as delivery vehicle for depot injectables comprising, for instance, steroids or antipsychotics [219]. Using a simple geometry limiting drug transport to one dimension, the diffusion and partitioning of piroxicam was characterized as a function of matrix (agarose and Pluronic F127) and pH of the aqueous gel phase utilizing expressions based on Ficks second law [221,237]. Changing pH from 4.0 to 7.4 appeared to have little impact on the diffusivity of piroxicam in the gel phase, however, a larger effect was observed on the distribution coefficient depending on the vehicles. This was attributed to medium polarity affecting the degree of piroxicam ionization. These proof-of-concept studies demonstrated the ability of UV imaging to detect and monitor small changes, however, the ability to monitor distribution of highly lipophilic studies remains to be demonstrated. The distribution of piroxicam upon injection of small volumes (3 μl) of aqueous and MCT solution into agarose gels was also assessed [237].

Sun et al. initially assessed the feasibility of UV imaging instrumentation to study the phase separation of in situ poly (lactide-*co*-glycolide acid) (PLGA) forming implants [225]. The PLGA was dissolved in 1-methyl-2-pyrrolidinone (NMP) or triacetin (TA) without model drug. The solutions were subsequently pipetted into a 2 mm wide cavity in the centre of an agarose gel. In this small-scale format, the effect of PLGA concentration (20 % and 40 % (w/w)) and type of cosolvent on the rate of phase separation was investigated at 550 nm. Using changes in absorbance or light intensity, slower phase separation with PLGA-TA than PLGA-NMP solutions was observed in line with existing literature on slow and fast phase separating systems. Interestingly, SEM and light microscopy studies showed that the agarose concentration had a significant impact on the morphology of the formed implants [225]. Concomitant UV imaging, Vis imaging and light microscopy were subsequently applied to monitor the in-situ formation of PLGA-NMP and PLGA-TA implants containing piroxicam or α-lactalbumin upon exposure to an aqueous medium in the form of 1.0 % (w/v) agarose gels [238]. The measurements were performed over 24 h using the so-called small-scale format, i.e., in 1 mm light path cuvettes holding the in-situ forming implants (20 μl preformulation), which were moved between the three measurement units. Implant formation was assessed using Vis imaging and light microscopy and initial drug release was quantified by UV imaging. α-Lactalbumin invoked an accelerated phase separation of the PLGA-solvent systems as compared to piroxicam, highlighting the interplay between (model) drug, polymer and cosolvent [238]. Recently, the initial (early time frame of 3 h) release of leuprolide acetate from in-situ forming PLGA-NMP implants was investigated by UV–Vis imaging [102]. Fig. 10 shows the schematic UV–Vis imaging setup applied and selected UV and Vis images recorded at selected time points. In contrast to previous studies, a larger imaging area of 25 × 25 mm^2 (and dual-wavelength capability) facilitated the injection of a dose and volume (3.0 mg of leuprolide acetate and 100 μl, respectively) comparable to a clinical setting. The study addressed the significance of different injection conditions and matrices applied for emulating the subcutaneous space [102]. Fig. 10B shows the effect of applying hyaluronic acid solution as the release matrix as compared to an agarose gel with or without an imbedded reservoir to define the geometry of the in situ forming implant. The increase in absorbance at 280 nm near the implants was due to the release and subsequent diffusion of the drug and represents a characteristic for UV imaging-based release studies. The visible wavelength (525 nm) was used for identifying the depot-matrix interface, which was subsequently applied to extract an estimate of implant swelling. The application of hyaluronic acid, a constituent of the extracellular matrix and a proposed subcutaneous tissue surrogate for *in vitro* release testing [239], led to lower leuprolide acetate release as compared to the release studies encompassing agarose gels. UV–Vis imaging was sufficiently sensitive to monitor the initial or burst release of leuprolide acetate from the long acting PLGA implant. Supplementary imaging measurements identified an interaction between the drug and the polyelectrolyte hyaluronic acid [102] (cf. Section 6), in addition to identifying the importance of the surrounding matrix on the swelling behaviour of the implants. Implant swelling and drug release have previously been reported to be affected by the interstitial pressure and compressive forces of the surrounding matrix [235].

In relation to injectables, dissolution studies of various insulins from compacts into agarose gel provided the following rank order: human insulin > bovine insulin > protamine insulin at pH 7.4 [223]. The dissolution of amorphous human insulin (pI ~ 5.4) was investigated at pH 3.0, 5.4 and 7.4. The dissolution rate was correlated to the apparent solubility of the peptide in the order pH 3.0 > 7.4 > 5.4. Surprisingly, the dissolution profiles exhibited different shapes in the stagnant system; a linear relationship between the amounts of human insulin dissolved and time was observed at pH 3.0 and 7.4, whereas at pH 5.4 the dissolution rate decreased with time consistent with $\sqrt{t}$ - kinetics. Based on "surface" insulin concentration measurements and in situ local pH measurements (the pH at the solid surface changed with time in the experiments performed at pH 3.0 ad 7.4) performed using the UV imaging instrumentation; the anomalous dissolution behaviour could be related to the ionization properties of insulin and the buffer capacity of the solution phase in the gel [223]. Jensen et al. further compared the release of insulin from drug loaded Sterotex implants into agarose gel by UV imaging [224]. The effect of drug load and implant porosity was assessed in a non-intrusive manner by imaging, however, the most striking result was the widely different release profiles obtained upon comparison to release profiles generated using another "gel sampling" method and an agitated phosphate buffer solution as the release media [224].

It should be noted that the prototypic release setups utilizing gels or stagnant solution phases discussed above work under non-sink conditions in contrast to what is normally recommended for dissolution and release testing. For the characterization of long acting injectables by UV–Vis imaging beyond the initial phase, incorporation of a convective contribution to drug transport is considered a necessity. To this end, Sun et al. applied a custom-made cell similar to the one depicted in Fig. 10A as a flow cell [240]. Piroxicam dissolved in 1-methyl-2-pyrrolidinone was injected into the flow cell being perfused with phosphate buffer at pH 7.4. UV imaging in combination with light microscopy and Raman spectroscopy was applied to monitor and document the initial local piroxicam supersaturation, precipitation occurring in the flow cell and subsequent drug dissolution. The powerful setup provided apparent drug concentrations and the parallel Raman measurements identified the solid form of the precipitated piroxicam [240]. The utility of such a setup for in situ forming suspensions or other depot type injectables can easily be envisioned. However,

the study also highlighted the sensitivity of such systems to small changes, e.g., with respect to hydrodynamic conditions. The simple alteration of the flow cell from a horizontal to an upright position fundamentally changed the outcome of the experiment due to the interplay between density and hydrodynamic conditions. This should be taken into consideration during the course of developing new *in vitro* release testing methods for injectables (and other formulation types). Even subtle changes may make comparison to work performed in other labs challenging. Similarly, the change of release medium and drug – matrix interactions discussed above may offer an opportunity to attain important new insights on formulations under development, but is likely to constitute a hindrance in a quality control setting (unless thoroughly characterized). The current UV–Vis imaging-based *in vitro* release testing methods for injectables, in their present form, cannot be expected to accurately model or simulate the entire *in vivo* release and absorption process upon, for instance, injection into subcutaneous or muscular tissue. The UV imaging setup rather lends itself to testing the importance individual physiological or physical chemical factors or processes. From a set of consecutive experiments involving UV imaging and other techniques, the entire release and absorption process may then be simulated. In its present form, UV imaging must be anticipated mainly to find use in early formulation screening rather than quality control and batch-to-batch release testing. Although the main area of use for UV imaging is aiding decision making in the early stages of formulation, due to its ability to produce a visualization of dissolution phenomena, it could have potential applications in quality control checks of finished formulations should they fail QC testing.

5.2. Miscellaneous formulations

As alluded to above, nicotine release from a transdermal patch was a first application of UV imaging [211]. As is probably the case for most of the applications discussed in this review, the study had the character of a feasibility study aiming to characterise UV imaging as a tool for performing *in vitro* drug release studies. Nicorette patch samples were mounted in a flow cell, the cell was filled with phosphate buffer, which was periodically replenished. The work mainly focussed on the analytical aspects of performing UV imaging measurements, e.g., calibration curve and LOQ. However, the release of nicotine as a function of time was quantified and found to adhere to Higuchi kinetics ($\sqrt{t}$ – kinetics) [211]. In relation to transdermal drug delivery, Fazili et al. investigated the permeation of ibuprofen over a silicone membrane in a 3D printed Franz type cell compatible with UV imaging [220]. The experimental setup facilitated real-time measurement of ibuprofen permeated to the acceptor phase. In the context of wound healing, Preem et al. studied the release of chloramphenicol from electrospun nanofiber mats using UV imaging [241] (Fig. 11). In line with previous studies, an agarose gel was applied as the release matrix assumed to reflect better the *in vivo* conditions as compared to a buffer solution. This setup allowed a qualitative comparison to antibacterial tests conducted on agar plates and a bioreporter disc diffusion assay. There was a considerable difference with respect to chloramphenicol release into phosphate buffer solution between mats made exclusively from polycaprolactone (PCL) and those comprising PCL and 2 % (w/v) polyethylene oxide (PEO). The faster drug release from the latter was attributed to the hydrophilic nature

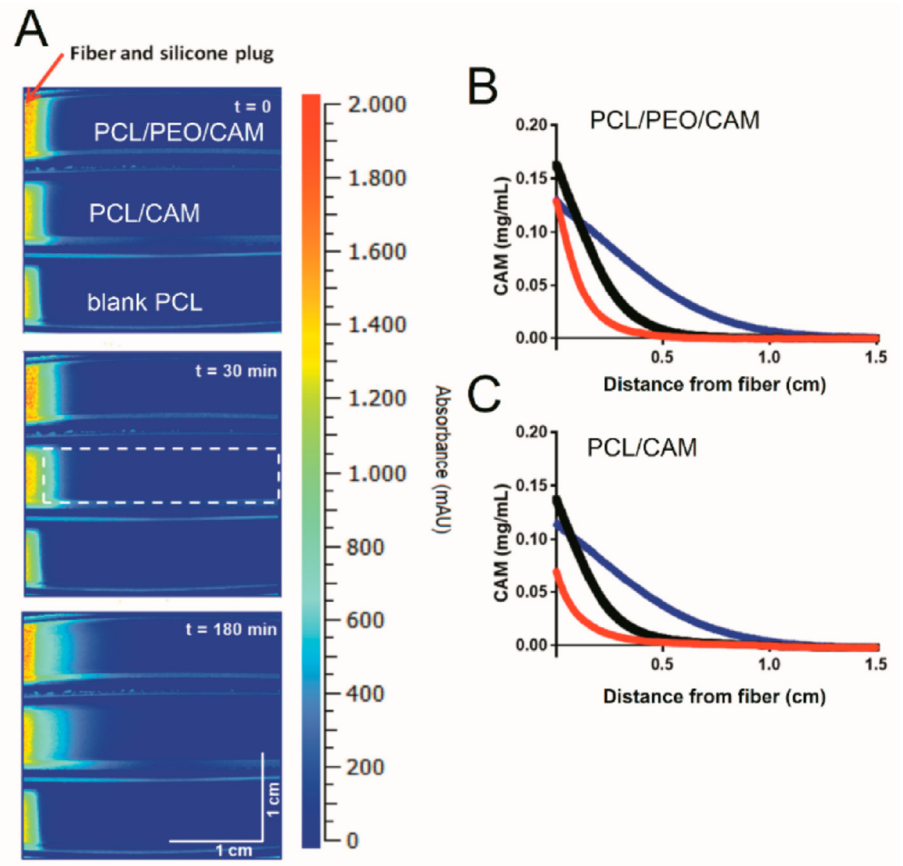

Fig. 11. (**A**) Representative images of CAM release from fibers and diffusion into 0.5% (*w*/*V*) agarose hydrogel at 37 °C. Top is PCL/PEO/CAM, middle is PCL/CAM and bottom is PCL/Blank fibers (control). The zone used for the quantification of the CAM absorbance is shown in the middle row at 30 min. Representative concentration-distance profiles for PCL/PEO/CAM (**B**) and PCL/CAM (**C**) fibers diffusing into 0.5% (*w*/*V*) agarose hydrogel at 37 °C. The red, black and blue line is for 0 min (immediately after starting the experiment), 30 min and 180 min, respectively. Key: CAM, chloramphenicol; PCL, polycaprolactone; PEO, polyethylene oxide. Reprinted from [241]. MDPI (Open Access).

of PEO. The same rank ordering, but with a much less pronounced difference, was observed upon chloramphenicol release into the hydrogels, indicating that the matrix constituted a diffusion barrier minimizing burst release effects [241]. He et al. designed HPMC-based buccal films containing the basic drug saquinavir (pK_a 7.1). With the aim of increasing the pH dependent solubility and release of saquinavir, the organic acids malic acid, citric acid or succinic acid were incorporated into the film matrix [242]. *In vitro* release testing at pH 6.8 showed that addition of an organic acid increased the release of saquinavir from the buccal films. Vis imaging was applied to probe the change in microenvironmental pH during drug release. The pH indicator bromothymol blue (pK_a 7.2) was dissolved in the phosphate buffer (pH 6.8) used for preparing the 0.5 % (w/v) agarose gel used as the release matrix. Saquinavir release from the films was initiated by placing the films on the gel in the imaging system. The local pH, or microenvironmental pH, was assessed by imaging at 610 nm where bromothymol blue has a pH dependent absorbance [242]. The apparent transient pH changes were the result of drug and excipient transport processes and the buffer capacity of the system. Further studies are, however, needed to assess how relevant the pH maps or images created are relative to the *in vivo* situation. However, the setup provides a simple approach for estimating local pH changes and potentially provides an indication on the importance of altering formulation parameters, i.e. pH modification.

6. Characterization of drug substances (and delivery systems)

The dissolution and release behavior of a drug substance is closely related to the physical chemical properties of the compound. Given the ability to monitor drug concentrations and concentration gradients, UV imaging may also be suited for characterization of physical chemical properties such as solubility, diffusion, partitioning, and binding or interaction phenomena in a spatially resolved manner.

According to the Noyes-Whitney model, the concentration of the dissolving substance at the solid surface is equal to the solubility. To this end, Lu and Li proposed a method for simultaneous measurement of drug solubility and diffusion coefficients based on fitting a numerical solution of Ficks second law to experimental drug concentration distributions determined from disk dissolution experiments performed under static conditions by UV imaging [193]. Satisfactory agreement to literature results was observed for the investigated model compounds carbamazepine and ibuprofen. UV imaging is also frequently denominated surface dissolution imaging. However, at least with the first generation instruments it has proved difficult to get good concentration measurements at the solid surface due to optical and instrument artefacts, cf. [141] and [99]. Thus, the approach of Lu and Li [193] deserve merit.

Diffusion, the transport of matter due to Brownian motion of molecules and a chemical potential gradient (concentration gradient) is one of the most important process in drug research. UV imaging provides an interesting approach to the study of drug diffusion properties. Methods such as dynamic light scattering, nuclear magnetic resonance and Taylor dispersion analysis are well suited for simple solutions [236,243] UV imaging, and other optical methods, are of particular interest in relation to more complex solutions and gels. Diffusion studies based on UV imaging have been performed in agarose gels [99,221,236], Pluronic F127 gel [222], composite gels of agarose and polyelectrolytes [237] and hyaluronic acid solution [102]. UV imaging diffusion measurements were sufficiently sensitive to capture the concentration and pH dependent self-association behavior of insulin attributed to the peptide monomers, dimers and hexamers [236]. A prerequisite for the use of UV imaging in diffusion studies is that natural

Table 3
Overview of UV imaging-based studies related to non-oral routes of administration and physical chemical characterization.

Drug/ excipient	Comments	Medium used	Reference
Nicotine transdermal patch	Static flow conditions	0.067 M phosphate buffer, pH 7.40	[211]
Piroxicam, human serum albumin	Effect of polymer concentration on diffusion	Pluronic F127 hydrogel	[222]
Piroxicam	Diffusion of drug from oil into hydrogel	Pluronic F127 hydrogel	[237]
Piroxicam	Influence of pH on drug diffusion and partitioning	Agarose and Pluronic F127 hydrogel	[221]
Saquinavir	Organic acid effects on pH and drug release from buccal films	Agarose gel	[242]
Chloramphenicol	IDR imaging from in situ ophthalmic gels		[245]
Insulin	Diffusion and self-association	Agarose gel	[236]
Insulin	Impact of pH on drug dissolution	Agarose gel	[223]
Insulin	Release from lipid implants, effect of drug load and release method	Agarose gel	[224]
α-lactalbumin, lysozyme, H-Ala-βNA, H-Lys-Lys-βNA	Effect of electrostatic interactions on diffusivity, composite gels	Agarose gel, hyaluronic acid, chondroitin sulfate	[244]
Lactide-co-glycolide acid (PLGA)	In situ PLGA implant formation	Agarose gel	[225]
Piroxicam and α-lactalbumin in lactide-co-glycolide acid (PLGA)	In situ PLGA implant formation and drug release	Agarose gel	[238]
Piroxicam	Supersaturation and subsequent precipitation of piroxicam	Phosphate buffer, pH 7.40	[240]
Chloramphenicol	Chloramphenicol release from loaded polycaprolactone (PCL) mats was investigated	Agarose gel	[241]
Leuprolide acetate	In situ PLGA implant formation and drug release upon injection	Agarose gel and hyaluronic acid	[102]
HPMC	Investigation of factors effecting the swelling of HPMC capsules	HCl, 0.01 m	[246]

convection due to density gradients can be adequately suppressed. Fortunately, the imaging approach itself constitutes a tool for detecting the occurrence of such phenomena as reported previously [99,126]. An additional prerequisite is that the matrix is sufficiently transparent. The diffusion studies are relatively easy to conduct. At University of Copenhagen, ~200 undergraduate students per year use the UV imaging setup for visualizing diffusion processes and determining diffusion coefficients during a 4 h lab exercise in the pharmacy program. Provided two different phases, i.e. two different gels or an oily and a gel phase are brought in contact with each other in the diffusion cell, UV imaging can also be used to visualize and assess partitioning effects. The distribution coefficients for the partitioning of piroxicam between MCT and aqueous gel phases were determined 11, 28. Along similar lines, Ye et al. investigated the role of electrostatic interactions as related to analyte diffusion in pure 0.5 % (w/v) agarose gel, 0.5 % (w/v) agarose gel containing 0.5% (w/v) chondroitin sulfate (CS), and 0.5% (w/v) agarose containing 0.5% (w/v) hyaluronic acid (HA) [244]. H-Ala-β-naphthylamide, H-Lys-Lys- β-naphthylamide, lysozyme and α-lactalbumin were selected as the model compounds. The incorporation of the negatively charged polyelectrolytes chondroitin sulfate and hyaluronic acid into the gel phase greatly reduced the apparent diffusion coefficients of the net positively charged molecules, whereas the diffusivity of α-lactalbumin was almost unaffected as compared to the diffusivities obtained in the neat 0.5 % agarose gel. The diffusivity of the cationic compounds was highly dependent on the ionic strength, with higher ionic strengths leading to a higher apparent diffusivity, indicating the effect of electrostatic interactions on apparent diffusivity [244]. A similar setup, identified the interaction of leuprolide acetate with hyaluronic acid [102] (Table 3). Such studies may be useful to assess the importance of drug physicochemical properties in relation to various drug release applications. UV imaging-based diffusion studies in gels are relatively well established, whereas further experiments are required to explore the wider applicability for assessing partition coefficients and interactions.

7. Instrument performance

UV dissolution imaging is interesting in formulation development due to its ability to monitor and relate physical changes to drug release rates, as discussed above (Section 4). The IDR and whole dose set-up of the UV dissolution process presents an interesting bridge between preformulation and compatibility studies and dosage form evaluation of used later in formulation development. Visualization is one of the key benefits of the UV imaging system with the measurement of drug concentrations in the immediate vicinity of the compacts or delivery system providing additional insights to the drug dissolution process [247]. UV dissolution imaging is complementary to many other imaging techniques, such as CARS, MRI, NMR imaging, XμT, FTIR imaging, NIR imaging, fluorescence imaging, and THz imaging, which provide information mainly related to the solid phase or the vehicle. A limitation of the UV/Vis imaging technique is the lack in chemical selectivity as compared to ATR-FTIR, Raman mapping and CARS and limited ability to monitor internal changes in internal structure such as the MRI and XμT.

Insights into the critical steps related to various applications start to emerge. A key issue is the establishment of best practices and protocols particularly in relation to data collection and data analysis to reduce sources of error. Approaches for characterizing instrument performance, for instance in relation to sensitivity, resolution, dynamic range and repeatability, are still under development [99,130,141,102 211]. The resolution is depending on the instrumentation used and the samples applied, but certainly larger than the pixel size ~ 30 μm for the Actipix D200 system [102] effectively limiting work with nano- and microparticles. The linear range observed is wavelength and matrix specific, and according to the experience of the authors in general less than for conventional UV/Vis spectrophotometers. Calibration curves should be prepared on the instrument used for the imaging measurements [99]. Having only one or a few wavelengths available, care should be exercised when attribution the measured absorbance to dissolved API or particulate or solid material scattering of blocking transmission of light. UV imaging has the unique advantage to offer qualitative data in the form of images of dissolution events and, thus, may still prove useful if accurate measurement of drug concentrations is not possible.

The relative simplicity of UV/Vis imaging technique in relation to its operation and data interpretation is likely to facilitate its uptake and use in formulation development labs. As USP dissolution methods are well established in QC and batch releases, it is unlikely that UV imaging will be used as a tool in these settings in the near future. The one sample at a time and lack of procedures for method suitability and instrument qualification are main obstacles.

8. Conclusion

The first applications of UV imaging in relation to dissolution and release testing appeared in 2010 [211,96]. Since, a number of studies have appeared, mainly in the area of intrinsic dissolution, form selection and drug-excipient interaction. Other studies have addressed drug release in relation to non-oral routes of administration or physical chemical characterization. Recently, with the advent of larger area imaging systems, whole dose studies related to tablets, capsules as well as injectables have started to occur. The key feature of UV imaging is related to the fact that most drug substances absorb light in the UV range, allowing drug concentrations and concentration gradients to be visualized and quantified at the surface of solid materials during dissolution or near the delivery vehicle during drug release. This opens for detailed insights into dissolution and release processes difficult to extract using conventional dissolution methods.

UV dissolution imaging ties in with at least two of the current trends in pharmaceutical sciences. One is miniaturization, to accommodate efficient characterization of new active molecules with the limited amounts of material available in the early stages of drug development. The miniaturisation comes in parallel with a high degree of analytical automation or a real-time analytical methods. Here the non-intrusive monitoring of the dissolution process makes UV imaging an attractive option for both the preformulation and formulation.

Another trend is the increasing application of high information content imaging modalities. The use of UV imaging to study pharmaceutical systems *in-vitro* is still at an early stage when compared to other imaging techniques such as CARS, MRI, NMR imaging, XμT, FTIR imaging, NIR imaging, fluorescence imaging, THz imaging and CLSM. The relative ease of operation and simple data analysis according to the Lambert-Beer law makes UV dissolution imaging an easily accessible imaging approach in formulation development. UV imaging is complementing most imaging techniques by monitoring mainly the solution phase. Some structural information on delivery vehicles may be obtained but in this sense UV imaging is generally much less selective. The microenvironment and structure of dosage forms characterized with respect to monitoring local pH changes, polymer swelling, peptide self-association and electrostatic interactions have been reported.

UV imaging is still an emerging technology but appears promising for drug dissolution research. Many published studies have the

character of method feasibility studies. This is likely to change in coming years. To this end, studies such as the danirixin [148] case is particularly encouraging bridging physical chemical characterization using UV imaging with clinical studies. Additional promising applications is the detailed elucidation of solid-state transformations possible by combining UV imaging with simultaneous in-situ Raman spectroscopy and the emerging whole dose applications.

9. Challenges and outlook

A range of small-scale dissolution methods for IDR determinations are available, most of which are capable of running multiple samples in parallel. In comparison to these, UV dissolution imaging is likely to a have lower throughput, but may also be associated with higher variability on the IDR values because quantification is relying on the suitability of the hydrodynamic model of the prevailing flow conditions and the image analysis. To what extent this limitation is counter balanced by the additional information generated by the images may depend on the specific application. Similar considerations may apply to the whole dose applications.

More work is needed for establishing method qualification and validation procedures for UV imaging. Media exhibiting high UV absorbance can also be problematic because of the limited linear range of the detector. Other challenges encountered in practical UV imaging are storage and analysis of large amounts of data captured. This is particularly challenging for sustained release formulations where prolonged monitoring is desirable. An unknown also, in relation to this area is the advances in UV imaging sensors.

The use of compendial dissolution testing instrumentation is generally endorsed and the proliferation of *in-vitro* release testing methods considered undesirable. However, the continued interest in developing new release testing methods most likely reflects an unmet need. With the current commercially available instrumentation, UV–Vis imaging is unlikely to replace the pharmacopeial methods as relates to QC, batch-to-batch, and biowaivers. The lack of multiplexing, or only one sample at a time, is a limitation, as is the lack of established instrument qualification procedures. UV imaging is more likely to find use in the area of formulation development shedding light on drug dissolution and release processes and mechanisms, i.e. method proliferation is likely to continue. Here the ability to rapidly design and make customized cells and holders compatible with the UV imaging instrumentation, e.g., by additive manufacturing [220,240] can be effectively exploited. It is envisioned that dedicated cells can be used to create systems emulating to a larger extent human physiology at the site of administration, which will be helpful in elucidating the rate limiting parameters controlling drug release, or to shed light on specific transport mechanisms.

UV/Vis imaging is a very versatile tool in drug research, the simplicity in terms of operation and (initial) data interpretation will favor continued use.

Declaration of Competing Interest

The authors declare that they have no known competing financial interests or personal relationships that could have appeared to influence the work reported in this paper.

Acknowledgements

The authors acknowledge the EPSRC DTP centre at the University of Huddersfield for funding Benedict Brown and the University of Huddersfield for funding Adam Ward and Zayeem Fazili. JØ would like to thank Professor David Goodall, Paraytec Ltd. for sharing his insights and the stimulating discussions.

References

[1] A. Fussell, E. Garbacik, H. Offerhaus, P. Kleinebudde, C. Strachan, In situ dissolution analysis using coherent anti-Stokes Raman scattering (CARS) and hyperspectral CARS microscopy, Eur. J. Pharm. Biopharm. 85 (3) (2013) 1141–1147.
[2] A. Paudel, D. Raijada, J. Rantanen, Raman spectroscopy in pharmaceutical product design, Adv. Drug Deliv. Rev. 89 (2015) 3–20, https://doi.org/10.1016/j.addr.2015.04.003 (Internet).
[3] G.P.S. Smith, C.M. McGoverin, S.J. Fraser, K.C. Gordon, Raman imaging of drug delivery systems, Adv. Drug Deliv. Rev. 89 (2015) 21–41, https://doi.org/10.1016/j.addr.2015.01.005 (Internet).
[4] J.C. Richardson, R.W. Bowtell, K. Mäder, C.D. Melia, Pharmaceutical applications of magnetic resonance imaging (MRI), Adv. Drug Deliv. Rev. 57 (8) (2005) 1191–1209.
[5] C.D. Melia, A.R. Rajabi-Siahboomi, R.W. Bowtell, Magnetic resonance imaging of controlled release pharmaceutical dosage forms, Pharm. Sci. Technol. Today 1 (1) (1998) 32–39.
[6] J.A. Zeitler, L.F. Gladden, In-vitro tomography and non-destructive imaging at depth of pharmaceutical solid dosage forms, Eur. J. Pharm. Biopharm. 71 (1) (2009) 2–22, https://doi.org/10.1016/j.ejpb.2008.08.012 (Internet).
[7] S.G. Kazarian, K.L.A. Chan, Applications of ATR-FTIR spectroscopic imaging to biomedical samples, Biochim. Biophys. Acta Biomembr. 1758 (7) (2006) 858–867.
[8] B. Van Eerdenbrugh, L.S. Taylor, Application of mid-IR spectroscopy for the characterization of pharmaceutical systems, Int. J. Pharm. 417 (1–2) (2011) 3–16, https://doi.org/10.1016/j.ijpharm.2010.12.011 (Internet).
[9] M. Jamrógiewicz, Application of the near-infrared spectroscopy in the pharmaceutical technology, J. Pharm. Biomed. Anal. 66 (2012) 1–10, https://doi.org/10.1016/j.jpba.2012.03.009 (Internet).
[10] J. Luypaert, D.L. Massart, H.Y. Vander, Near-infrared spectroscopy applications in pharmaceutical analysis, Talanta 72 (3) (2007) 865–883.
[11] A.M. Pena, X. Chen, I.J. Pence, T. Bornschlögl, S. Jeong, S. Grégoire, et al., Imaging and quantifying drug delivery in skin – Part 2: Fluorescence andvibrational spectroscopic imaging methods, Adv. Drug Deliv. Rev. 153 (2020) 147–168.
[12] J.A. Zeitler, Y. Shen, C. Baker, P.F. Taday, M. Pepper, T. Rades, Analysis of Coating Structures and Interfaces in Solid Oral Dosage Forms by Three Dimensional Terahertz Pulsed Imaging Available from: J. Pharm. Sci. 96 (2) (2007) 330–340.
[13] P. Bawuah, J.A. Zeitler, Advances in terahertz time-domain spectroscopy of pharmaceutical solids: A review, TrAC, Trends Anal. Chem. 139 (2021) 116272, https://doi.org/10.1016/j.trac.2021.116272 (Internet).
[14] S.R. Pygall, J. Whetstone, P. Timmins, C.D. Melia, Pharmaceutical applications of confocal laser scanning microscopy: The physical characterisation of pharmaceutical systems, Adv. Drug Deliv. Rev. 59 (14) (2007) 1434–1452.
[15] Y. Sun, J. Østergaard, Application of UV Imaging in Formulation Development, Pharm. Res. 34 (5) (2017) 929–940.
[16] J. Østergaard, UV imaging in pharmaceutical analysis, J. Pharm. Biomed. Anal. 147 (2018) 140–148, https://doi.org/10.1016/j.jpba.2017.07.055 (Internet).
[17] M. Windbergs, M. Jurna, H.L. Offerhaus, J.L. Herek, P. Kleinebudde, C.J. Strachan, Chemical imaging of oral solid dosage forms and changes upon dissolution using coherent anti-Stokes Raman scattering microscopy, Anal. Chem. 81 (6) (2009) 2085–2091.
[18] M. Jurna, M. Windbergs, C.J. Strachan, L. Hartsuiker, C. Otto, P. Kleinebudde, et al., Coherent anti-Stokes Raman scattering microscopy to monitor drug dissolution in different oral pharmaceutical tablets, J Innov Opt Health Sci. 2 (01) (2009) 37–43.
[19] L. Zhang, M.J. Henson, S.S. Sekulic, Multivariate data analysis for Raman imaging of a model pharmaceutical tablet, Anal. Chim. Acta 545 (2) (2005) 262–278.
[20] S. Šašić, D.A. Clark, J.C. Mitchell, M.J. Snowden, A comparison of Raman chemical images produced by univariate and multivariate data processing—a simulation with an example from pharmaceutical practice, Analyst. 129 (11) (2004) 1001–1007.
[21] P.Y. Sacré, C. De Bleye, P.F. Chavez, L. Netchacovitch, P. Hubert, E. Ziemons, Data processing of vibrational chemical imaging for pharmaceutical applications, J. Pharm. Biomed. Anal. 101 (2014) 123–140, https://doi.org/10.1016/j.jpba.2014.04.012 (Internet).
[22] S. Šašić, S. Mehrens, Raman chemical mapping of low-content active pharmaceutical ingredient formulations. III. Statistically optimized sampling and detection of polymorphic forms in tablets on stability, Anal. Chem. 84 (2) (2012) 1019–1025.
[23] Structure and behaviour in hydrophilic matrix sustained release dosage forms: 2. NMR-imaging studies of dimensional changes in the gel layer and core of HPMC tablets undergoing hydration. J. Control Release 31(2) (1994).
[24] M. Ashraf, V.L. Iuorno, D. Coffin-Beach, C.A. Evans, L.L. Augsburger, A novel nuclear magnetic resonance (NMR) imaging method for measuring the water front penetration rate in hydrophilic polymer matrix capsule plugs and its role in drug release, Pharm. Res. 11 (5) (1994) 733–737.
[25] R. Bowtell, J.C. Sharp, A. Peters, P. Mansfield, A.R. Rajabi-Siahboomi, M.C. Davies, et al., NMR microscopy of hydrating hydrophilic matrix

pharmaceutical tablets Available from Magn. Reson. Imaging 12 (2) (1994) 361–364. https://www.sciencedirect.com/science/article/pii/0730725X94915563.
[26] A. Djemai, L.F. Gladden, J. Booth, R.S. Kittlety, P.R. Gellert, MRI investigation of hydration and heterogeneous degradation of aliphatic polyesters derived from lactic and glycolic acids: A controlled drug delivery device, Magn. Reson. Imaging 19 (3–4) (2001) 521–523.
[27] N. Mawla, S. Hanley, K. Walton, W. Kaialy, T. Hussain, A. Ward, et al., Imaging of the effect of alcohol-containing media on the performance of hypromellose hydrophilic matrix tablets: Comparison of direct compression and regular grades of polymer, Pharmaceutics. 12 (9) (2020) 1–20.
[28] G. Tomer, M.D. Mantle, L.F. Gladden, J.M. Newton, Measuring water distribution in extrudates using magnetic resonance imaging (MRI), Int. J. Pharm. 189 (1) (1999) 19–28.
[29] A.R. Rajabi-Siahboomi, R.W. Bowtell, P. Mansfield, M.C. Davies, C.D. Melia, Structure and Behavior in Hydrophilic Matrix Sustained Release Dosage Forms: 4. Studies of Water Mobility and Diffusion Coefficients in the Gel Layer of HPMC Tablets Using NMR Imaging, Pharm. Res. 13 (3) (1996) 376–380, https://doi.org/10.1023/A:1016084224084.
[30] C.A. Fyfe, A.I. Blazek, Investigation of hydrogel formation from hydroxypropylmethylcellulose (HPMC) by NMR spectroscopy and NMR imaging techniques, Macromolecules 30 (20) (1997) 6230–6237.
[31] T.M. Hyde, L.F. Gladden, Simultaneous measurement of water and polymer concentration profiles during swelling of poly(ethylene oxide) using magnetic resonance imaging, Polymer (Guildf). 39 (4) (1998) 811–819.
[32] P. Marshall, J.E.M. Snaar, Y.L. Ng, R.W. Bowtell, F.C. Hampson, P.W. Dettmar, et al., Localised mapping of water movement and hydration inside a developing bioadhesive bond, J. Control. Release 95 (3) (2004) 435–446.
[33] M. Shapiro, M. Ann, S. Gravina, controlled release Magnetic resonance imaging of an oral gastrointestinal-therapeutic-system (GITS) tablet water penetration, J. Control. Release 38 (1996) 123–127.
[34] N. Sommier, P. Porion, P. Evesque, B. Leclerc, P. Tchoreloff, G. Couarraze, Magnetic resonance imaging investigation of the mixing-segregation process in a pharmaceutical blender, Int. J. Pharm. 222 (2) (2001) 243–258.
[35] J. Tritt-Goc, J. Kowalczuk, In situ, real time observation of the disintegration of paracetamol tablets in aqueous solution by magnetic resonance imaging, Eur. J. Pharm. Sci. 15 (4) (2002) 341–346.
[36] B.J. Fahie, A. Nangia, S.K. Chopra, C.A. Fyfe, H. Grondey, A. Blazek, Use of NMR imaging in the optimization of a compression-coated regulated release system, J. Control. Release 51 (2–3) (1998) 179–184.
[37] J.C.D. Sutch, A.C. Ross, W. Köckenberger, R.W. Bowtell, R.J. MacRae, H.N.E. Stevens, et al., Investigating the coating-dependent release mechanism of a pulsatile capsule using NMR microscopy, J. Control. Release 92 (3) (2003) 341–347.
[38] G. Nebgen, D. Gross, V. Lehmann, F. Müller, 1H-NMR microscopy of tablets, J. Pharm. Sci. 84 (3) (1995) 283–291.
[39] M.A. Ansari, F. Stepanek, Formation of hollow core granules by fluid bed in situ melt granulation: modelling and experiments, Int. J. Pharm. 321 (1–2) (2006) 108–116.
[40] C.-Y. Yang, X.-Y. Fu, Development and validation of a material-labeling method for powder process characterization using X-ray computed tomography, Powder Technol. 146 (1–2) (2004) 10–19.
[41] D.H. Phillips, J.J. Lannutti, Measuring physical density with X-ray computed tomography, Ndt E Int. 30 (6) (1997) 339–350.
[42] I.C. Sinka, S.F. Burch, J.H. Tweed, J.C. Cunningham, Measurement of density variations in tablets using X-ray computed tomography, Int. J. Pharm. 271 (1–2) (2004) 215–224.
[43] P.R. Laity, K. Asare-Addo, F. Sweeney, E. Šupuk, B.R. Conway, Using small-angle X-ray scattering to investigate the compaction behaviour of a granulated clay, Appl. Clay Sci. 108 (2015) 149–164.
[44] P.R. Laity, M.D. Mantle, L.F. Gladden, R.E. Cameron, Magnetic resonance imaging and X-ray microtomography studies of a gel-forming tablet formulation, Eur. J. Pharm. Biopharm. 74 (1) (2010) 109–119.
[45] M. Alshafiee, M.K. Aljammal, D. Markl, A. Ward, K. Walton, L. Blunt, et al., Hot-melt extrusion process impact on polymer choice of glyburide solid dispersions: The effect of wettability and dissolution, Int. J. Pharm. 559 (2019) 245–254.
[46] Y. Ozeki, Y. Watanabe, S. Inoue, K. Danjo, Comparison of the compression characteristics between new one-step dry-coated tablets (OSDRC) and dry-coated tablets (DC), Int. J. Pharm. 259 (1–2) (2003) 69–77.
[47] L. Farber, G. Tardos, J.N. Michaels, Use of X-ray tomography to study the porosity and morphology of granules, Powder Technol. 132 (1) (2003) 57–63.
[48] X. Fu, J.A. Elliott, A.C. Bentham, B.C. Hancock, R.E. Cameron, Application of X-ray Microtomography and Image Processing to the Investigation of a Compacted Granular System, Part. Part. Syst. Char. 23 (3–4) (2006) 229–236.
[49] E.I. Nep, K. Asare-Addo, M.U. Ghori, B.R. Conway, A.M. Smith, Starch-free grewia gum matrices: Compaction, swelling, erosion and drug release behaviour, Int. J. Pharm. 496 (2) (2015) 689–698.
[50] D. Traini, G. Loreti, A.S. Jones, P.M. Young, X-ray computed microtomography for the study of modified release systems, Microsc. Anal. 123 (2008) 13.
[51] P.S. Wray, G.S. Clarke, S.G. Kazarian, Dissolution of tablet-in-tablet formulations studied with ATR-FTIR spectroscopic imaging, Eur. J. Pharm. Sci. 48 (4–5) (2013) 748–757.
[52] F.D. Zahoor, K.T. Mader, P. Timmins, J. Brown, C. Sammon, Investigation of within-tablet dynamics for extended release of a poorly soluble basic drug from hydrophilic matrix tablets using ATR–FTIR imaging, Mol. Pharm. 17 (4) (2020) 1090–1099.
[53] H. Hifumi, A.V. Ewing, S.G. Kazarian, ATR-FTIR spectroscopic imaging to study the drying and dissolution of pharmaceutical polymer-based films, Int. J. Pharm. 515 (1–2) (2016) 57–68.
[54] W. Li, A. Woldu, L. Araba, D. Winstead, Determination of water penetration and drug concentration profiles in HPMC-based matrix tablets by near infrared chemical imaging, J. Pharm. Sci. 99 (7) (2010) 3081–3088.
[55] P. Avalle, S.R. Pygall, N. Gower, A. Midwinter, The use of in situ near infrared spectroscopy to provide mechanistic insights into gel layer development in HPMC hydrophilic matrices, Eur. J. Pharm. Sci. 43 (5) (2011) 400–408.
[56] S.D. Novak, E. Šporar, S. Baumgartner, F. Vrečer, Characterization of physicochemical properties of hydroxypropyl methylcellulose (HPMC) type 2208 and their influence on prolonged drug release from matrix tablets, J. Pharm. Biomed. Anal. 66 (2012) 136–143.
[57] J.I. Jérez Rozo, A. Zarow, B. Zhou, R. Pinal, Z. Iqbal, R.J. Romañach, Complementary near-infrared and raman chemical imaging of pharmaceutical thin films, J. Pharm. Sci. 100 (11) (2011) 4888–4895.
[58] J.M. Prats-Montalbán, J.I. Jerez-Rozo, R.J. Romañach, A. Ferrer, MIA and NIR chemical imaging for pharmaceutical product characterization, Chemom. Intell. Lab. Syst. 117 (2012) 240–249.
[59] M. Erdoğan, Y. Yagci, Ö. Pekcan, Slow release of trapped homopolymers from a swelling polymeric gel: a fluorescence study, J Macromol Sci Part B. 47 (5) (2008) 942–954.
[60] Ö. Pekcan, Y. Yilmaz, Flourescence method to study gelation swelling and drying processes in gels formed by solution free radical compolymerization, Gels. Springer (1996) 89–97.
[61] Ö. Pekcan, Ş. Uğur, Y. Yılmaz, Real-time monitoring of swelling and dissolution of poly (methyl methacrylate) discs using fluorescence probes, Polymer (Guildf). 38 (9) (1997) 2183–2189.
[62] O. Tari, O. Pekcan, Modelling of swelling by the fluorescence technique in kappa carrageenan gels, in: AIP Conference Proceedings, American Institute of Physics, 2011, pp. 470–475.
[63] A.J. Fitzgerald, B.E. Cole, P.F. Taday, Nondestructive analysis of tablet coating thicknesses using terahertz pulsed imaging, J. Pharm. Sci. 94 (1) (2005) 177–183.
[64] L. Ho, R. Müller, M. Römer, K.C. Gordon, J. Heinämäki, P. Kleinebudde, et al., Analysis of sustained-release tablet film coats using terahertz pulsed imaging Available from J. Control Release 119 (3) (2007) 253–261. https://www.sciencedirect.com/science/article/pii/S0168365907001460.
[65] J.A. Spencer, Z. Gao, T. Moore, L.F. Buhse, P.F. Taday, D.A. Newnham, et al., Delayed release tablet dissolution related to coating thickness by terahertz pulsed image mapping, J. Pharm. Sci. 97 (4) (2008) 1543–1550.
[66] H. Lin, Y. Dong, D. Markl, B.M. Williams, Y. Zheng, Y. Shen, et al., Measurement of the intertablet coating uniformity of a pharmaceutical pan coating process with combined terahertz and optical coherence tomography in-line sensing, J. Pharm. Sci. 106 (4) (2017) 1075–1084.
[67] H. Lin, R.K. May, M.J. Evans, S. Zhong, L.F. Gladden, Y. Shen, et al., Impact of processing conditions on inter-tablet coating thickness variations measured by terahertz in-line sensing, J. Pharm. Sci. 104 (8) (2015) 2513–2522.
[68] Y.C. Shen, P.F. Taday, D.A. Newnham, M. Pepper, Chemical mapping using reflection terahertz pulsed imaging, Semicond. Sci. Technol. 20 (7) (2005) S254.
[69] R.P. Cogdill, S.M. Short, R. Forcht, Z. Shi, Y. Shen, P.F. Taday, et al., An efficient method-development strategy for quantitative chemical imaging using terahertz pulse spectroscopy, J. Pharm. Innov. 1 (1) (2006) 63–75.
[70] R. Palermo, R.P. Cogdill, S.M. Short, J.K. Drennen III, P.F. Taday, Density mapping and chemical component calibration development of four-component compacts via terahertz pulsed imaging, J. Pharm. Biomed. Anal. 46 (1) (2008) 36–44.
[71] Y.-C. Shen, P.F. Taday, Development and application of terahertz pulsed imaging for nondestructive inspection of pharmaceutical tablet, IEEE J. Sel. Top. Quantum Electron. 14 (2) (2008) 407–415.
[72] A. Novikova, D. Markl, J.A. Zeitler, T. Rades, C.S. Leopold, A non-destructive method for quality control of the pellet distribution within a MUPS tablet by terahertz pulsed imaging, Eur. J. Pharm. Sci. 111 (2018) 549–555.
[73] P. Bawuah, D. Markl, A. Turner, M. Evans, A. Portieri, D. Farrell, et al., A Fast and Non-destructive Terahertz Dissolution Assay for Immediate Release Tablets, J. Pharm. Sci. (2020).
[74] P. Bawuah, A.P. Mendia, P. Silfsten, P. Pääkkönen, T. Ervasti, J. Ketolainen, et al., Detection of porosity of pharmaceutical compacts by terahertz radiation transmission and light reflection measurement techniques, Int. J. Pharm. 465 (1–2) (2014) 70–76.
[75] P. Bawuah, P. Silfsten, T. Ervasti, J. Ketolainen, J.A. Zeitler, K.-E. Peiponen, Non-contact weight measurement of flat-faced pharmaceutical tablets using terahertz transmission pulse delay measurements, Int. J. Pharm. 476 (1–2) (2014) 16–22.
[76] D. Markl, P. Bawuah, C. Ridgway, S. van den Ban, D.J. Goodwin, J. Ketolainen, et al., Fast and non-destructive pore structure analysis using terahertz time-domain spectroscopy, Int. J. Pharm. 537 (1–2) (2018) 102–110, https://doi.org/10.1016/j.ijpharm.2017.12.029 (Internet).
[77] G.S. Bajwa, K. Hoebler, C. Sammon, P. Timmins, C.D. Melia, Microstructural imaging of early gel layer formation in HPMC matrices, J. Pharm. Sci. 95 (10) (2006) 2145–2157.

[78] S.R. Pygall, S. Kujawinski, P. Timmins, C.D. Melia, The suitability of tris (hydroxylmethyl) aminomethane (THAM) as a buffering system for hydroxypropyl methylcellulose (HPMC) hydrophilic matrices containing a weak acid drug, Int. J. Pharm. 387 (1–2) (2010) 93–102.

[79] L.M. Mason, M.D. Campiñez, S.R. Pygall, J.C. Burley, P. Gupta, D.E. Storey, et al., The influence of polymer content on early gel-layer formation in HPMC matrices: the use of CLSM visualisation to identify the percolation threshold, Eur. J. Pharm. Biopharm. 94 (2015) 485–492.

[80] H.D. Williams, K.P. Nott, D.A. Barrett, R. Ward, I.J. Hardy, C.D. Melia, Drug release from HPMC matrices in milk and fat-rich emulsions, J. Pharm. Sci. 100 (11) (2011) 4823–4835.

[81] H.D. Williams, R. Ward, I.J. Hardy, C.D. Melia, The extended release properties of HPMC matrices in the presence of dietary sugars, J. Control. Release 138 (3) (2009) 251–259.

[82] S. Svanbäck, H. Ehlers, J. Yliruusi, Optical microscopy as a comparative analytical technique for single-particle dissolution studies, Int. J. Pharm. 469 (1) (2014) 10–16.

[83] S. Svanbäck, H. Ehlers, O. Antikainen, J. Yliruusi, On-Chip optofluidic single-particle method for rapid microscale equilibrium solubility screening of biologically active substances, Anal. Chem. 87 (10) (2015) 5041–5045.

[84] S. Svanbäck, H. Ehlers, O. Antikainen, J. Yliruusi, High-speed intrinsic dissolution rate in one minute using the single-particle intrinsic dissolution rate method, Anal. Chem. 87 (21) (2015) 11058–11064.

[85] J. Østergaard, UV/Vis Spectrophotometry and UV Imaging, in: A. Müllertz, Y. Perrie, T. Rades (Eds.), Analytical Techniques in the Pharmaceutical Sciences, Springer New York, New York, NY, 2016, pp. 3–27. Available from: https://doi.org/10.1007/978-1-4939-4029-5_1 (Internet).

[86] S. Görög, Ultraviolet-Visible Spectrophotometry in Pharmaceutical Analysis, CRC Press, 1995. Available from: https://www.taylorfrancis.com/books/9781351085878 (Internet).

[87] D.S. Hage, J.D. Carr, Analytical chemistry and quantitative analysis, Prentice Hall, Boston, 2011.

[88] Paraytec. Paraytec Ltd. Home Page.. [cited 2021 Apr 7]. Available from: http://paraytec.com (Internet).

[89] Glenn Tyrrell, UV-Shifted Silicon Devices for Imaging and Detection, Photonics Spectra (2006).

[90] A. Lahav, A. Fenigstein, A. Strum, M. Haemek, N. Beach, Backside illuminated (BSI) complementary metal-oxidesemiconductor (CMOS) image sensors, in: D. Durini (Ed.), High Performance Silicon Imaging - Fundamentals and Applications of CMOS and CCD Sensors, second ed., Elsevier, 2020, pp. 95–117.

[91] K. Kaufmann, CMOS Technology for Scientific Imaging, Spectroscopy 25(7) (2010).

[92] M. Kulp, P.L. Urban, M. Kaljurand, E.T. Bergström, D.M. Goodall, Visualization of electrophoretically mediated in-capillary reactions using a complementary metal oxide semiconductor-based absorbance detector, Anal. Chim. Acta 570 (1) (2006) 1–7.

[93] P.L. Urban, D.M. Goodall, E.T. Bergström, N.C. Bruce, Electrophoretic assay for penicillinase: substrate specificity screening by parallel CE with an active pixel sensor, Electrophoresis 28 (12) (2007) 1926–1936.

[94] P.L. Urban, E.T. Bergström, D.M. Goodall, S. Narayanaswamy, N.C. Bruce, Electrophoretic method for assessment of substrate promiscuity of a heterogeneous biocatalyst using an area imaging ultraviolet detector, Analyst. 132 (10) (2007) 979–982.

[95] P.L. Urban, D.M. Goodall, E.T. Bergström, N.C. Bruce, Electrophoretically mediated microanalysis of a nicotinamide adenine dinucleotide-dependent enzyme and its facile multiplexing using an active pixel sensor UV detector, J. Chromatogr. A 1162 (2) (2007) 132–140.

[96] S. Wren, J. Lenke, Pharmaceutical dissolution and UV imaging, Am. Lab. 43 (2) (2011) 33.

[97] J.P. Boetker, M. Savolainen, V. Koradia, F. Tian, T. Rades, A. Müllertz, et al., Insights into the early dissolution events of amlodipine using UV imaging and Raman spectroscopy, Mol. Pharm. 8 (4) (2011) 1372–1380.

[98] W.L. Hulse, J. Gray, R.T. Forbes, A discriminatory intrinsic dissolution study using UV area imaging analysis to gain additional insights into the dissolution behaviour of active pharmaceutical ingredients, Int. J. Pharm. 434 (1–2) (2012) 133–139, https://doi.org/10.1016/j.ijpharm.2012.05.023 (Internet).

[99] S.S. Jensen, H. Jensen, D.M. Goodall, J. Østergaard, Performance characteristics of UV imaging instrumentation for diffusion, dissolution and release testing studies, J. Pharm. Biomed. Anal. 131 (2016) 113–123, https://doi.org/10.1016/j.jpba.2016.08.018 (Internet).

[100] Pion. https://pion-inc.com/scientific-instruments/dissolution/surface-imaging/sdi2.

[101] Paraytec. https://www.paraytec.com/actipix-imaging-detectors/.

[102] Z. Li, H. Mu, S.W. Larsen, H. Jensen, J. Østergaard, Initial Leuprolide Acetate Release from Poly (d, l-lactide-co-glycolide) in Situ Forming Implants as Studied by Ultraviolet-Visible Imaging, Mol. Pharm. 17 (12) (2020) 4522–4532.

[103] K.G. Nelson, A.C. Shah, Evaluation of a convective diffusion drug dissolution rate model, J. Pharm. Sci. 64 (9) (1975) 1518–1520.

[104] A. Ward, K. Walton, S. Stoycheva, M. Wallis, A. Adebisi, E. Nep, et al., The use of visible and UV dissolution imaging for the assessment of propranolol hydrochloride in liquisolid compacts of Sesamum radiatum gum, J Drug Deliv Sci Technol. 56 (2020) 101511.

[105] K. Asare-Addo, M. Alshafiee, K. Walton, A. Ward, A.M. Totea, S. Taheri, et al., Effect of preparation method on the surface properties and UV imaging of indomethacin solid dispersions, Eur. J. Pharm. Biopharm. 137 (January) (2019) 148–163, https://doi.org/10.1016/j.ejpb.2019.03.002 (Internet).

[106] A. Ward, K. Walton, N. Mawla, W. Kaialy, L. Liu, P. Timmins, et al., Development of a novel method utilising dissolution imaging for the measurement of swelling behaviour in hydrophilic matrices, Int. J. Pharm. X. 1 (2019) 100013.

[107] L.I. Chambers, H. Grohganz, H. Palmelund, K. Löbmann, T. Rades, O.M. Musa, et al., Predictive identification of co-formers in co-amorphous systems, Eur. J. Pharm. Sci. 157 (2021) 105636.

[108] Sirius Analytical Instruments. SDi2 Instruction Manual, 2017.

[109] E.S. Kostewicz, B. Abrahamsson, M. Brewster, J. Brouwers, J. Butler, S. Carlert, et al., In vitro models for the prediction of in vivo performance of oral dosage forms, Eur. J. Pharm. Sci. 57 (2014) 342–366.

[110] M. Kuentz, Analytical technologies for real-time drug dissolution and precipitation testing on a small scale, J. Pharm. Pharmacol. 67 (2) (2015) 143–159.

[111] C.A.S. Bergström, K. Box, R. Holm, W. Matthews, M. McAllister, A. Müllertz, et al., Biorelevant intrinsic dissolution profiling in early drug development: Fundamental, methodological, and industrial aspects, Eur. J. Pharm. Biopharm. 139 (October 2018) (2019) 101–114, https://doi.org/10.1016/j.ejpb.2019.03.011 (Internet).

[112] A. Avdeef, O. Tsinman, Miniaturized rotating disk intrinsic dissolution rate measurement: Effects of buffer capacity in comparisons to traditional wood's apparatus, Pharm. Res. 25 (11) (2008) 2613–2627.

[113] C.M. Berger, O. Tsinman, D. Voloboy, D. Lipp, S. Stones, A. Avdeef, Miniaturized intrinsic dissolution rate (mini-idr) measurement of griseofulvin and carbamazepine, Disso Tech. 11 (2007) 39–41.

[114] A.M. Persson, K. Baumann, L.-O. Sundelöf, W. Lindberg, A. Sokolowski, C. Pettersson, Design and characterization of a new miniaturized rotating disk equipment for in vitro dissolution rate studies, J. Pharm. Sci. 97 (8) (2008) 3344–3355.

[115] K. Tsinman, A. Avdeef, O. Tsinman, D. Voloboy, Powder dissolution method for estimating rotating disk intrinsic dissolution rates of low solubility drugs, Pharm. Res. 26 (9) (2009) 2093–2100.

[116] T. Gravestock, K. Box, J. Comer, E. Frake, S. Judge, R. Ruiz, The, "GI dissolution" method: a low volume, in vitro apparatus for assessing the dissolution/precipitation behaviour of an active pharmaceutical ingredient under biorelevant conditions, Anal. Methods 3 (3) (2011) 560–567.

[117] S. Klein, V. Shah, The mini paddle apparatus—a useful tool in the early developmental stage? Experiences with immediate release dosage forms, Dissolution Technol. 13 (4) (2006) 6–11.

[118] S. Klein, V.P. Shah, A standardized mini paddle apparatus as an alternative to the standard paddle, Aaps Pharmscitech. 9 (4) (2008) 1179–1184.

[119] A. Shanbhag, S. Rabel, E. Nauka, G. Casadevall, P. Shivanand, G. Eichenbaum, et al., Method for screening of solid dispersion formulations of low-solubility compounds—miniaturization and automation of solvent casting and dissolution testing, Int. J. Pharm. 351 (1–2) (2008) 209–218.

[120] J. Alsenz, E. Haenel, A. Anedda, P. Du Castel, G. Cirelli, Miniaturized INtrinsic DISsolution Screening (MINDISS) assay for preformulation, Eur. J. Pharm. Sci. 87 (2016) 3–13, https://doi.org/10.1016/j.ejps.2015.09.008 (Internet).

[121] S. Klein, N.L. Buchanan, C.M. Buchanan, Miniaturized transfer models to predict the precipitation of poorly soluble weak bases upon entry into the small intestine, Aaps Pharmscitech. 13 (4) (2012) 1230–1235.

[122] T. Yamashita, S. Ozaki, I. Kushida, Solvent shift method for anti-precipitant screening of poorly soluble drugs using biorelevant medium and dimethyl sulfoxide, Int. J. Pharm. 419 (1–2) (2011) 170–174.

[123] K. Tsinman, O. Tsinman, Dissolution-Permeability Apparatus with Integrated In Situ Concentration Monitoring of both Donor and Receiver Compartments, in: AAPS annual meeting, 2013.

[124] J. Alsenz, E.V.A. Meister, E. Haenel, Development of a partially automated solubility screening (PASS) assay for early drug development Available from: J. Pharm. Sci. 96 (7) (2007) 1748–1762.

[125] N. Wyttenbach, J. Alsenz, O. Grassmann, Miniaturized assay for solubility and residual solid screening (SORESOS) in early drug development, Pharm. Res. 24 (5) (2007) 888–898.

[126] J. Østergaard, F. Ye, J. Rantanen, A. Yaghmur, S.W. Larsen, C. Larsen, et al., Monitoring lidocaine single-crystal dissolution by ultraviolet imaging Available from J. Pharm. Sci.. 100 (8) (2011) 3405–3410. https://linkinghub.elsevier.com/retrieve/pii/S0022354915319936.

[127] G.E. Amidon, W.I. Higuchi, N.F.H. Ho, Theoretical and experimental studies of transport of micelle-solubilized solutes, J. Pharm. Sci. 71 (1) (1982) 77–84.

[128] L. Yu, G.L. Amidon, Analytical solutions to mass transfer, Transp. Process. Pharm. Syst. 23 (1999).

[129] L. Yu, A.S. Carlin, G.L. Amidon, A.S. Hussain, Feasibility studies of utilizing disk intrinsic dissolution rate to classify drugs, Int. J. Pharm. 270 (1–2) (2004) 221–227.

[130] K. Etherson, C. Dunn, W. Matthews, H. Pamelund, C. Barragat, N. Sanderson, et al., An interlaboratory investigation of intrinsic dissolution rate determination using surface dissolution, Eur. J. Pharm. Biopharm. 150 (2020) 24–32, https://doi.org/10.1016/j.ejpb.2020.02.005 (Internet).

[131] A. Dokoumetzidis, P. Macheras, A century of dissolution research: From Noyes and Whitney to the Biopharmaceutics Classification System, Int. J. Pharm. 321 (1–2) (2006) 1–11.

[132] K.G. Nelson, A.C. Shah, Convective diffusion model for a transport-controlled dissolution rate process, J. Pharm. Sci. 64 (4) (1975) 610–614.
[133] J. Lenke, Two dimensional orthogonal imaging of laminar fluid flow across API surface: insight into dosage concentration inside GI lumen and permeability, in: The Electronic Conference on Pharmaceutical Sciences: ECPS20112011, 2012.
[134] N. Qiao, K. Wang, W. Schlindwein, A. Davies, M. Li, In situ monitoring of carbamazepine-nicotinamide cocrystal intrinsic dissolution behaviour, Eur. J. Pharm. Biopharm. 83 (3) (2013) 415–426, https://doi.org/10.1016/j.ejpb.2012.10.005 (Internet).
[135] S. Gordon, K. Naelapää, J. Rantanen, A. Selen, A. Müllertz, J. Ostergaard, Real-time dissolution behavior of furosemide in biorelevant media as determined by UV imaging, Pharm. Dev. Technol. 18 (6) (2013) 1407–1416.
[136] J. Østergaard, J.X. Wu, K. Naelapää, J.P. Boetker, H. Jensen, J. Rantanen, Simultaneous UV Imaging and Raman Spectroscopy for the Measurement of Solvent-Mediated Phase Transformations During Dissolution Testing Available from J. Pharm. Sci. 103 (4) (2014) 1149–1156. https://linkinghub.elsevier.com/retrieve/pii/S0022354915306328.
[137] Colombo S, Brisander M, Haglöf J, Sjövall P, Andersson P, Østergaard J, et al. Matrix effects in nilotinib formulations with pH-responsive polymer produced by carbon dioxide-mediated precipitation. Int. J. Pharm. 2015;494 (1):205–17. Doi: 10.1016/j.ijpharm.2015.08.031
[138] H. Ueda, J. Peter Bøtker, M. Edinger, K. Löbmann, H. Grohganz, A. Müllertz, et al., Formulation of co-amorphous systems from naproxen and naproxen sodium and in situ monitoring of physicochemical state changes during dissolution testing by Raman spectroscopy, Int. J. Pharm. 587 (June) (2020), https://doi.org/10.1016/j.ijpharm.2020.119662 (Internet).
[139] A. Ward, K. Walton, K. Box, J. Østergaard, L.J. Gillie, B.R. Conway, et al., Variable-focus microscopy and UV surface dissolution imaging as complementary techniques in intrinsic dissolution rate determination, Int. J. Pharm. 530 (1–2) (2017) 139–144.
[140] B. Brown, Z. Fazili, A. Ward, K. Walton, L. Blunt, J. Østergaard, et al., An investigation of drug compact topography as relates to intrinsic dissolution rates determined by dissolution imaging, J. Drug Deliv. Sci. Technol. (2020).
[141] J.P. Boetker, J. Rantanen, T. Rades, A. Müllertz, J. Østergaard, H. Jensen, A new approach to dissolution testing by UV imaging and finite element simulations, Pharm. Res. 30 (5) (2013) 1328–1337.
[142] M. Li, N. Qiao, K. Wang, Influence of sodium lauryl sulfate and Tween 80 on carbamazepine-nicotinamide cocrystal solubility and dissolution behaviour, Pharmaceutics 5 (4) (2013) 508–524.
[143] A. Niederquell, M. Kuentz, Biorelevant dissolution of poorly soluble weak acids studied by UV imaging reveals ranges of fractal-like kinetics, Int. J. Pharm. 463 (1) (2014) 38–49, https://doi.org/10.1016/j.ijpharm.2013.12.049 (Internet).
[144] J. Østergaard, H. Jensen, S.W. Larsen, C. Larsen, J. Lenke, Microenvironmental pH measurement during sodium naproxenate dissolution in acidic medium by UV/vis imaging, J. Pharm. Biomed. Anal. 100 (2014) 290–293, https://doi.org/10.1016/j.jpba.2014.08.014 (Internet).
[145] A.T.M. Serajuddin, Salt formation to improve drug solubility, Adv. Drug Deliv. Rev. 59 (7) (2007) 603–616.
[146] D.P. Elder, R. Holm, H.L. de Diego, Use of pharmaceutical salts and cocrystals to address the issue of poor solubility, Int. J. Pharm. 453 (1) (2013) 88–100.
[147] R.J. Bastin, M.J. Bowker, B.J. Slater, Salt selection and optimisation procedures for pharmaceutical new chemical entities, Org. Process Res. Dev. 4 (5) (2000) 427–435.
[148] J.C. Bloomer, C. Ambery, B.E. Miller, P. Connolly, H. Garden, N. Henley, et al., Identification and characterisation of a salt form of Danirixin with reduced pharmacokinetic variability in patient populations, Eur. J. Pharm. Biopharm. 117 (2017) 224–231, https://doi.org/10.1016/j.ejpb.2017.03.023.
[149] M. Ramirez, S.E. David, C.H. Schwalbe, K. Asare-Addo, B.R. Conway, P. Timmins, Crystal packing arrangement, chain conformation, and physicochemical properties of gemfibrozil amine salts, Cryst. Growth Des. 17 (7) (2017) 3743–3750.
[150] S.B.E. Andersson, C. Alvebratt, J. Bevernage, D. Bonneau, Mathews C da Costa, R. Dattani, et al., Interlaboratory Validation of Small-Scale Solubility and Dissolution Measurements of Poorly Water-Soluble Drugs, J. Pharm. Sci. 105 (9) (2016) 2864–2872.
[151] L.H. Nielsen, S. Gordon, J.P. Pajander, J. Østergaard, T. Rades, A. Müllertz, Biorelevant characterisation of amorphous furosemide salt exhibits conversion to a furosemide hydrate during dissolution, Int. J. Pharm. 457 (1) (2013) 14–24, https://doi.org/10.1016/j.ijpharm.2013.08.029 (Internet).
[152] L.H. Nielsen, S. Gordon, R. Holm, A. Selen, T. Rades, A. Müllertz, Preparation of an amorphous sodium furosemide salt improves solubility and dissolution rate and leads to a faster Tmax after oral dosing to rats, Eur. J. Pharm. Biopharm. 85 (3) (2013) 942–951.
[153] W. Kirchmeyer, N. Wyttenbach, J. Alsenz, M. Kuentz, Influence of excipients on solvent-mediated hydrate formation of piroxicam studied by dynamic imaging and fractal analysis, Cryst. Growth Des. 15 (10) (2015) 5002–5010.
[154] S. Aleandri, M. Schönenberger, A. Niederquell, M. Kuentz, Temperature-induced surface effects on drug nanosuspensions, Pharm. Res. 35 (3) (2018) 1–11.
[155] P. Macheras, A. Iliadis, G. Melagraki, A reaction limited in vivo dissolution model for the study of drug absorption: Towards a new paradigm for the biopharmaceutic classification of drugs, Eur. J. Pharm. Sci. 117 (2018) 98–106.
[156] R. Abreu-Villela, M. Schönenberger, I. Caraballo, M. Kuentz, Early stages of drug crystallization from amorphous solid dispersion via fractal analysis based on chemical imaging, Eur. J. Pharm. Biopharm. 133 (2018) 122–130.
[157] R. Abreu-Villela, M. Kuentz, I. Caraballo, Benefits of Fractal Approaches in Solid Dosage Form Development, Pharm. Res. 36 (11) (2019) 1–13.
[158] E.O. Kissi, H. Grohganz, K. Löbmann, M.T. Ruggiero, J.A. Zeitler, T. Rades, Glass-transition temperature of the β-relaxation as the major predictive parameter for recrystallization of neat amorphous drugs, J. Phys. Chem. B 122 (10) (2018) 2803–2808.
[159] M. Rams-Baron, R. Jachowicz, E. Boldyreva, D. Zhou, W. Jamroz, M. Paluch, Physical Instability: A Key Problem of Amorphous Drugs, Amorphous Drugs. Springer (2018) 107–157.
[160] D.J. Berry, J.W. Steed, Pharmaceutical cocrystals, salts and multicomponent systems; intermolecular interactions and property based design, Adv. Drug Deliv. Rev. 117 (2017) 3–24.
[161] A.M. Healy, Z.A. Worku, D. Kumar, A.M. Madi, Pharmaceutical solvates, hydrates and amorphous forms: A special emphasis on cocrystals, Adv. Drug Deliv. Rev. 117 (2017) 25–46.
[162] S. Khodadadi, G.M.H. Meesters, Amorphous APIs: Improved Release, Preparation, Characterization, in: Particles and Nanoparticles in Pharmaceutical Products, Springer, 2018, pp. 329–346.
[163] M. Adobes-Vidal, F.M. Maddar, D. Momotenko, L.P. Hughes, S.A.C. Wren, L.N. Poloni, et al., Face-discriminating dissolution kinetics of furosemide single crystals: in situ three-dimensional multi-microscopy and modeling, Cryst. Growth Des. 16 (8) (2016) 4421–4429.
[164] F.M. Maddar, M. Adobes-Vidal, L.P. Hughes, S.A.C. Wren, P.R. Unwin, Dissolution of Bicalutamide Single Crystals in Aqueous Solution: Significance of Evolving Topography in Accelerating Face-Specific Kinetics, Cryst. Growth Des. 17 (10) (2017) 5108–5116.
[165] M. Najib, R.B. Hammond, T. Mahmud, T. Izumi, Impact of Structural Binding Energies on Dissolution Rates for Single Faceted-Crystals, Cryst. Growth Des. 21 (3) (2021) 1482–1495.
[166] T.T.H. Nguyen, R.B. Hammond, K.J. Roberts, I. Marziano, G. Nichols, Precision measurement of the growth rate and mechanism of ibuprofen 001 and 011 as a function of crystallization environment, CrystEngComm 16 (21) (2014) 4568–4586.
[167] B.Y. Shekunov, D.J.W. Grant, R.J. Latham, J.N. Sherwood, In situ optical interferometric studies of the growth and dissolution behavior of paracetamol (acetaminophen) crystals. 3. Influence of growth in the presence of p-acetoxyacetanilide, J. Phys. Chem. B 101 (44) (1997) 9107–9112.
[168] L de O. Macedo, E.J. Barbosa, R. Löbenberg, N.A. Bou-Chacra, Anti-inflammatory drug nanocrystals: state of art and regulatory perspective. Eur. J. Pharm. Sci. (2020) 105654.
[169] F. Fontana, P. Figueiredo, P. Zhang, J.T. Hirvonen, D. Liu, H.A. Santos, Production of pure drug nanocrystals and nano co-crystals by confinement methods, Adv. Drug Deliv. Rev. 131 (2018) 3–21.
[170] A. Sarnes, J. Østergaard, S.S. Jensen, J. Aaltonen, J. Rantanen, J. Hirvonen, et al., Dissolution study of nanocrystal powders of a poorly soluble drug by UV imaging and channel flow methods, Eur. J. Pharm. Sci. 50 (3–4) (2013) 511–519, https://doi.org/10.1016/j.ejps.2013.08.030 (Internet).
[171] R.P. Dixit, S.P. Puthli, Oral strip technology: overview and future potential, J. Control. Release 139 (2) (2009) 94–107.
[172] S.M. Krull, R. Susarla, A. Afolabi, M. Li, Y. Ying, Z. Iqbal, et al., Polymer strip films as a robust, surfactant-free platform for delivery of BCS Class II drug nanoparticles, Int. J. Pharm. 489 (1–2) (2015) 45–57.
[173] A.F. Borges, C. Silva, J.F.J. Coelho, S. Simões, Oral films: current status and future perspectives: I—galenical development and quality attributes, J. Control. Release 206 (2015) 1–19.
[174] B.D. Kevadiya, L. Zhang, R.N. Davé, Sustained release of poorly water-soluble drug from hydrophilic polymeric film sandwiched between hydrophobic layers, AAPS PharmSciTech. 19 (6) (2018) 2572–2584.
[175] B.D. Kevadiya, M. Barvaliya, L. Zhang, A. Anovadiya, H. Brahmbhatt, P. Paul, et al., Fenofibrate nanocrystals embedded in oral strip-films for bioavailability enhancement, Bioengineering 5 (1) (2018) 1–17.
[176] J. Pajander, S. Baldursdottir, J. Rantanen, J. Østergaard, Behaviour of HPMC compacts investigated using UV-imaging, Int. J. Pharm. 427 (2) (2012) 345–353, https://doi.org/10.1016/j.ijpharm.2012.02.034 (Internet).
[177] B. Arafat, M. Wojsz, A. Isreb, R.T. Forbes, M. Isreb, W. Ahmed, et al., Tablet fragmentation without a disintegrant: A novel design approach for accelerating disintegration and drug release from 3D printed cellulosic tablets, Eur. J. Pharm. Sci. 2018 (118) (2017) 191–199.
[178] D.M. Schachter, J. Xiong, G.C. Tirol, Solid state NMR perspective of drug–polymer solid solutions: a model system based on poly (ethylene oxide), Int. J. Pharm. 281 (1–2) (2004) 89–101.
[179] A. Newman, K. Nagapudi, R. Wenslow, Amorphous solid dispersions: a robust platform to address bioavailability challenges, Ther. Deliv. 6 (2) (2015) 247–261.
[180] T.W.Y. Lee, N.A. Boersen, H.W. Hui, S.F. Chow, K.Y. Wan, H.L.A. Chow, Delivery of poorly soluble compounds by amorphous solid dispersions, Curr. Pharm. Des. 20 (3) (2014) 303–324.
[181] A. Paudel, M. Geppi, G. Van den Mooter, Structural and dynamic properties of amorphous solid dispersions: the role of solid-state nuclear magnetic resonance spectroscopy and relaxometry, J. Pharm. Sci. 103 (9) (2014) 2635–2662.

[182] K. Kawakami, K. Sato, M. Fukushima, A. Miyazaki, Y. Yamamura, S. Sakuma, Phase separation of supersaturated solution created from amorphous solid dispersions: Relevance to oral absorption, Eur. J. Pharm. Biopharm. 132 (2018) 146–156.
[183] A. Smeets, R. Koekoekx, C. Clasen, G. Van den Mooter, Amorphous solid dispersions of darunavir: Comparison between spray drying and electrospraying, Eur. J. Pharm. Biopharm. 130 (2018) 96–107.
[184] L.-P. Ruan, B.-Y. Yu, G.-M. Fu, D. Zhu, Improving the solubility of ampelopsin by solid dispersions and inclusion complexes, J. Pharm. Biomed. Anal. 38 (3) (2005) 457–464.
[185] D.N. Nguyen, L. Palangetic, C. Clasen, G. Van den Mooter, One-step production of darunavir solid dispersion nanoparticles coated with enteric polymers using electrospraying, J. Pharm. Pharmacol. 68 (5) (2016) 625–633.
[186] N. Ogawa, T. Hiramatsu, R. Suzuki, R. Okamoto, K. Shibagaki, K. Fujita, et al., Improvement in the water solubility of drugs with a solid dispersion system by spray drying and hot-melt extrusion with using the amphiphilic polyvinyl caprolactam-polyvinyl acetate-polyethylene glycol graft copolymer and d-mannitol, Eur. J. Pharm. Sci. 111 (2018) 205–214.
[187] T. Van Duong, G. Van den Mooter, The role of the carrier in the formulation of pharmaceutical solid dispersions. Part II: amorphous carriers, Expert Opin Drug Deliv. 13 (12) (2016) 1681–1694.
[188] N. Gautschi, P. Van Hoogevest, M. Kuentz, Amorphous drug dispersions with mono- and diacyl lecithin: On molecular categorization of their feasibility and UV dissolution imaging, Int. J. Pharm. 491 (1–2) (2015) 218–230, https://doi.org/10.1016/j.ijpharm.2015.06.039 (Internet).
[189] P. Zarmpi, T. Flanagan, E. Meehan, J. Mann, N. Fotaki, Surface dissolution UV imaging for characterization of superdisintegrants and their impact on drug dissolution, Int. J. Pharm. 577 (January) (2020), https://doi.org/10.1016/j.ijpharm.2020.119080 (Internet).
[190] C.M. Long, K. Tang, H. Chokshi, N. Fotaki, Surface Dissolution UV Imaging for Investigation of Dissolution of Poorly Soluble Drugs and Their Amorphous Formulation, AAPS PharmSciTech. 20 (3) (2019).
[191] T.N. Hiew, Alaudin M.I. Bin, S.M. Chua, P.W.S. Heng, A study of the impact of excipient shielding on initial drug release using UV imaging, Int. J. Pharm. 553 (1–2) (2018) 229–237, https://doi.org/10.1016/j.ijpharm.2018.10.040 (Internet).
[192] P. Madelung, P. Bertelsen, J. Jacobsen, A. Müllertz, J. Østergaard, Dissolution enhancement of griseofulvin from griseofulvin-sodium dodecyl sulfate discs investigated by UV imaging, J. Drug Deliv. Sci. Technol. 39 (2017) 516–522, https://doi.org/10.1016/j.jddst.2017.05.010 (Internet).
[193] Y. Lu, M. Li, Simultaneous Rapid Determination of the Solubility and Diffusion Coefficients of a Poorly Water-Soluble Drug Based on a Novel UV Imaging System Available from J. Pharm. Sci. 105 (1) (2016) 131–138. https://linkinghub.elsevier.com/retrieve/pii/S0022354915001367.
[194] K. Asare-Addo, K. Walton, A. Ward, A.M. Totea, S. Taheri, M. Alshafiee, et al., Direct imaging of the dissolution of salt forms of a carboxylic acid drug, Int. J. Pharm. 551 (1–2) (2018) 290–299, https://doi.org/10.1016/j.ijpharm.2018.09.048 (Internet).
[195] A. Nokhodchi, S. Raja, P. Patel, K. Asare-Addo, The role of oral controlled release matrix tablets in drug delivery systems, BioImpacts BI. 2 (4) (2012) 175.
[196] P. Timmins, D. Desai, W. Chen, P. Wray, J. Brown, S. Hanley, Advances in mechanistic understanding of release rate control mechanisms of extended-release hydrophilic matrix tablets, Ther. Deliv. 7 (8) (2016) 553–572.
[197] H.E. Huber, L.B. Dale, G.L. Christenson, Utilization of hydrophilic gums for the control of drug release from tablet formulations I. Disintegration and dissolution behavior, J. Pharm. Sci. 55 (9) (1966) 974–976.
[198] D.A. Alderman, A review of cellulose ethers in hydrophilic matrices for oral controlled-release dosage forms, Int. J. Pharm. Tech. Prod. Mfr. 5 (3) (1984) 1–9.
[199] K. Asare-Addo, B.R. Conway, H. Larhrib, M. Levina, A.R. Rajabi-Siahboomi, J. Tetteh, et al., The effect of pH and ionic strength of dissolution media on in-vitro release of two model drugs of different solubilities from HPMC matrices, Colloids Surfaces B Biointerfaces. 111 (2013) 384–391.
[200] M. Levina, A.R. Rajabi-Siahboomi, The influence of excipients on drug release from hydroxypropyl methylcellulose matrices, J. Pharm. Sci. 93 (11) (2004) 2746–2754.
[201] A. Ward, B. Brown, K. Walton, P. Timmins, B.R. Conway, K. Asare-Addo, Application of Focus Variation Microscopy and Dissolution Imaging in Understanding the Behaviour of Hydrophilic Matrices, Pharmaceutics 12 (12) (2020) 1162.
[202] M. Levina, H. Vuong, A.R. Rajabi-Siahboomi, The influence of hydro-alcoholic media on hypromellose matrix systems, Drug Dev. Ind. Pharm. 33 (10) (2007) 1125–1134.
[203] M. Roberts, M. Cespi, J.L. Ford, A.M. Dyas, J. Downing, L.G. Martini, et al., Influence of ethanol on aspirin release from hypromellose matrices, Int. J. Pharm. 332 (1–2) (2007) 31–37.
[204] N. Kavanagh, O.I. Corrigan, Swelling and erosion properties of hydroxypropylmethylcellulose (Hypromellose) matrices—influence of agitation rate and dissolution medium composition, Int. J. Pharm. 279 (1–2) (2004) 141–152.
[205] A. Nokhodchi, C.M. Hentzschel, C.S. Leopold, Drug release from liquisolid systems: speed it up, slow it down, Expert Opin. Drug Deliv. 8 (2) (2011) 191–205.
[206] D.M. Koller, G. Hannesschläger, M. Leitner, J.G. Khinast, Non-destructive analysis of tablet coatings with optical coherence tomography, Eur. J. Pharm. Sci. 44 (1–2) (2011) 142–148.
[207] M.H. Gaunø, T. Vilhelmsen, C.C. Larsen, J.P. Boetker, J. Wittendorff, J. Rantanen, et al., Real-time in vitro dissolution of 5-aminosalicylic acid from single ethyl cellulose coated extrudates studied by UV imaging, J. Pharm. Biomed. Anal. 83 (2013) 49–56, https://doi.org/10.1016/j.jpba.2013.04.028 (Internet).
[208] F. Alqahtani, P. Belton, A. Ward, K. Asare-Addo, S. Qi, An investigation into the use of low quantities of functional additives to control drug release from hot melt extruded solid dispersions for poorly soluble drug delivery, Int. J. Pharm. 579 (2020) 119172.
[209] P. Zarmpi, T. Flanagan, E. Meehan, J. Mann, J. Østergaard, N. Fotaki, Biopharmaceutical implications of excipient variability on drug dissolution from immediate release products, Eur. J. Pharm. Biopharm. 154 (10) (2020) 195–209, https://doi.org/10.1016/j.ejpb.2020.07.014 (Internet).
[210] B. Arafat, N. Qinna, M. Cieszynska, R.T. Forbes, M.A. Alhnan, Tailored on demand anti-coagulant dosing: an in vitro and in vivo evaluation of 3D printed purpose-designed oral dosage forms, Eur. J. Pharm. Biopharm. 128 (2018) 282–289.
[211] J. Østergaard, E. Meng-Lund, S.W. Larsen, C. Larsen, K. Petersson, J. Lenke, et al., Real-time UV imaging of nicotine release from transdermal patch, Pharm. Res. 27 (12) (2010) 2614–2623.
[212] S.N.F. D'Souza, Injectables, in: S. Klein (Ed.), In vitro drug release testing of special dosage forms, John Wiley & sons Ltd, Hoboken, NJ, USA, 2020, pp. 57–85.
[213] M.N. Martinez, M.J. Rathbone, D. Burgess, M. Huynh, Breakout session summary from AAPS/CRS joint workshop on critical variables in the in vitro and in vivo performance of parenteral sustained release products, J. Control. Release 142 (1) (2010) 2–7.
[214] C.K. Brown, H.D. Friedel, A.R. Barker, L.F. Buhse, S. Keitel, T.L. Cecil, et al., FIP/AAPS joint workshop report: dissolution/in vitro release testing of novel/special dosage forms, Springer, 2011.
[215] S.S. D'Souza, P.P. DeLuca, Methods to assess in vitro drug release from injectable polymeric particulate systems, Pharm. Res. 23 (3) (2006) 460–474.
[216] S.W. Larsen, J. Østergaard, A. Yaghmur, H. Jensen, C. Larsen, Use of in vitro release models in the design of sustained and localized drug delivery systems for subcutaneous and intra-articular administration, J. Drug Deliv. Sci. Technol. 23 (4) (2013) 315–324, https://doi.org/10.1016/S1773-2247(13)50048-7 (Internet).
[217] M.T. Dadhaniya, O. Prakash Sharma, C.M. Gohel, J.P. Mehta, Current approaches for in vitro drug release study of long acting parenteral formulations, Curr. Drug Deliv. 12 (3) (2015) 256–270.
[218] J. Shen, D.J. Burgess, In vitro–in vivo correlation for complex non-oral drug products: where do we stand?, J Control. Release 219 (2015) 644–651.
[219] C. Larsen, S.W. Larsen, H. Jensen, A. Yaghmur, J. Østergaard, Role of in vitro release models in formulation development and quality control of parenteral depots, Expert Opin Drug. Deliv. 6 (12) (2009) 1283–1295.
[220] Z. Fazili, A. Ward, K. Walton, L. Blunt, K. Asare-Addo, Design and development of a novel fused filament fabrication (FFF) 3D printed diffusion cell with UV imaging capabilities to characterise permeation in pharmaceutical formulations, Eur. J. Pharm. Biopharm. 152 (2020) 202–209.
[221] F. Ye, S.W. Larsen, A. Yaghmur, H. Jensen, C. Larsen, J. Østergaard, Real-time UV imaging of piroxicam diffusion and distribution from oil solutions into gels mimicking the subcutaneous matrix, Eur. J. Pharm. Sci. 46 (1–2) (2012) 72–78, https://doi.org/10.1016/j.ejps.2012.02.011 (Internet).
[222] F. Ye, A. Yaghmur, H. Jensen, S.W. Larsen, C. Larsen, J. Østergaard, Real-time UV imaging of drug diffusion and release from Pluronic F127 hydrogels, Eur. J. Pharm. Sci. 43 (4) (2011) 236–243, https://doi.org/10.1016/j.ejps.2011.04.015 (Internet).
[223] S.S. Jensen, H. Jensen, C. Cornett, E.H. Møller, J. Østergaard, Real-time UV imaging identifies the role of pH in insulin dissolution behavior in hydrogel-based subcutaneous tissue surrogate, Eur. J. Pharm. Sci. 69 (2015) 26–36, https://doi.org/10.1016/j.ejps.2014.12.015 (Internet).
[224] S.S. Jensen, H. Jensen, E.H. Møller, C. Cornett, F. Siepmann, J. Siepmann, et al., In vitro release studies of insulin from lipid implants in solution and in a hydrogel matrix mimicking the subcutis, Eur. J. Pharm. Sci. 81 (2015) 103–112, https://doi.org/10.1016/j.ejps.2015.10.011 (Internet).
[225] Y. Sun, H. Jensen, N.J. Petersen, S.W. Larsen, J. Østergaard, Phase separation of in situ forming poly (lactide-co-glycolide acid) implants investigated using a hydrogel-based subcutaneous tissue surrogate and UV–vis imaging, J. Pharm. Biomed. Anal. 145 (2017) 682–691, https://doi.org/10.1016/j.jpba.2017.07.056 (Internet).
[226] D. Klose, N. Azaroual, F. Siepmann, G. Vermeersch, J. Siepmann, Towards more realistic in vitro release measurement techniques for biodegradable microparticles, Pharm. Res. 26 (3) (2009) 691–699.
[227] D.H. Leung, Y. Kapoor, C. Alleyne, E. Walsh, A. Leithead, B. Habulihaz, et al., Development of a convenient in vitro gel diffusion model for predicting the in vivo performance of subcutaneous parenteral formulations of large and small molecules, AAPS PharmSciTech. 18 (6) (2017) 2203–2213.
[228] U. Gietz, T. Arvinte, E. Mader, P. Oroszlan, H.P. Merkle, Sustained release of injectable zinc-recombinant hirudin suspensions: development and validation of in vitro release model, Eur. J. Pharm. Biopharm. 45 (3) (1998) 259–264.

[229] J. Kožák, M. Rabišková, A. Lamprecht, In-vitro drug release testing of parenteral formulations via an agarose gel envelope to closer mimic tissue firmness, Int. J. Pharm. 594 (2021) 120142.
[230] S. Allababidi, J.C. Shah, Kinetics and mechanism of release from glyceryl monostearate-based implants: Evaluation of release in a gel simulating in vivo implantation, J. Pharm. Sci. 87 (6) (1998) 738–744.
[231] B. Semmling, S. Nagel, K. Sternberg, W. Weitschies, A. Seidlitz, Impact of different tissue-simulating hydrogel compartments on in vitro release and distribution from drug-eluting stents, Eur. J. Pharm. Biopharm. 87 (3) (2014) 570–578.
[232] T.H.H. Thi, F. Chai, S. Leprêtre, N. Blanchemain, B. Martel, F. Siepmann, et al., Bone implants modified with cyclodextrin: Study of drug release in bulk fluid and into agarose gel, Int. J. Pharm. 400 (1–2) (2010) 74–85.
[233] R. Peschka, C. Dennehy, F.C. Szoka Jr, A simple in vitro model to study the release kinetics of liposome encapsulated material, J. Control. Release 56 (1–3) (1998) 41–51.
[234] C. Hernandez, N. Gawlik, M. Goss, H. Zhou, S. Jeganathan, D. Gilbert, et al., Macroporous acrylamide phantoms improve prediction of in vivo performance of in situ forming implants, J. Control. Release 243 (2016) 225–231.
[235] R.B. Patel, L. Solorio, H. Wu, T. Krupka, A.A. Exner, Effect of injection site on in situ implant formation and drug release in vivo, J. Control. Release 147 (3) (2010) 350–358.
[236] S.S. Jensen, H. Jensen, C. Cornett, E.H. Møller, J. Østergaard, Insulin diffusion and self-association characterized by real-time UV imaging and Taylor dispersion analysis, J. Pharm. Biomed. Anal. 92 (2014) 203–210, https://doi.org/10.1016/j.jpba.2014.01.022 (Internet).
[237] F. Ye, S.W. Larsen, A. Yaghmur, H. Jensen, C. Larsen, J. Østergaard, Drug release into hydrogel-based subcutaneous surrogates studied by UV imaging, J. Pharm. Biomed. Anal. 71 (2012) 27–34, https://doi.org/10.1016/j.jpba.2012.07.024 (Internet).
[238] Y. Sun, H. Jensen, N.J. Petersen, S.W. Larsen, J. Østergaard, Concomitant monitoring of implant formation and drug release of in situ forming poly (lactide-co-glycolide acid) implants in a hydrogel matrix mimicking the subcutis using UV–vis imaging, J. Pharm. Biomed. Anal. 150 (2018) 95–106, https://doi.org/10.1016/j.jpba.2017.11.065 (Internet).
[239] H.M. Kinnunen, V. Sharma, L.R. Contreras-Rojas, Y. Yu, C. Alleman, A. Sreedhara, et al., A novel in vitro method to model the fate of subcutaneously administered biopharmaceuticals and associated formulation components, J. Control. Release 214 (2015) 94–102.
[240] Y. Sun, A. Chapman, S.W. Larsen, H. Jensen, N.J. Petersen, D.M. Goodall, et al., UV-vis Imaging of Piroxicam Supersaturation, Precipitation, and Dissolution in a Flow-Through Setup, Anal. Chem. 90 (11) (2018) 6413–6418.
[241] L. Preem, F. Bock, M. Hinnu, M. Putrinš, K. Sagor, T. Tenson, et al., Monitoring of antimicrobial drug chloramphenicol release from electrospun nano-and microfiber mats using UV imaging and bacterial bioreporters, Pharmaceutics. 11 (9) (2019) 1–19.
[242] S. He, J. Østergaard, M. Ashna, C.U. Nielsen, J. Jacobsen, H. Mu, Microenvironmental pH modifying films for buccal delivery of saquinavir: Effects of organic acids on pH and drug release in vitro, Int. J. Pharm. 585 (6) (2020), https://doi.org/10.1016/j.ijpharm.2020.119567 (Internet).
[243] F. Ye, H. Jensen, S.W. Larsen, A. Yaghmur, C. Larsen, J. Østergaard, Measurement of drug diffusivities in pharmaceutical solvents using Taylor dispersion analysis, J. Pharm. Biomed. Anal. 61 (2012) 176–183.
[244] F. Ye, S. Baldursdottir, S. Hvidt, H. Jensen, S.W. Larsen, A. Yaghmur, et al., Role of Electrostatic Interactions on the Transport of Druglike Molecules in Hydrogel-Based Articular Cartilage Mimics: Implications for Drug Delivery, Mol. Pharm. 13 (3) (2016) 819–828.
[245] J.-X. Chen, Z. Guo, H.-Y. Li, L. Wu, Z.-G. He, R.-F. Hu, et al., Real-time UV imaging of chloramphenicol intrinsic dissolution characteristics from ophthalmic in situ gel, Yao xue xue bao= Acta Pharm. Sin. 48 (7) (2013) 1156–1163.
[246] C. Tong, Z. Wang, Y. Zhog, M. Zhen, Investigation of factors effected dissolution variations of hydroxypropyl methylcellulose capsule, African J. Pharm. Pharmacol. 7 (22) (2013) 1501–1511.
[247] J. Østergaard, J. Lenke, S.S. Jensen, Y. Sun, F. Ye, UV imaging for in vitro dissolution and release studies: Initial experiences, Dissolution Technol. 21 (4) (2014) 27–38.